

# Light- and bias-induced metastabilities in $\text{Cu}(\text{In, Ga})\text{Se}_2$ based solar cells caused by the $(V_{\text{Se}}-V_{\text{Cu}})$ vacancy complex

Stephan Lany and Alex Zunger

Citation: *Journal of Applied Physics* **100**, 113725 (2006); doi: 10.1063/1.2388256

View online: <http://dx.doi.org/10.1063/1.2388256>

View Table of Contents: <http://aip.scitation.org/toc/jap/100/11>

Published by the American Institute of Physics


---

## Articles you may be interested in

Bulk and metastable defects in  $\text{CuIn}_{1-x}\text{Ga}_x\text{Se}_2$  thin films using drive-level capacitance profiling

*Journal of Applied Physics* **95**, (2004); 10.1063/1.1633982

---



Small Conferences. BIG Ideas.

Applied Physics  
Reviews

SAVE THE DATE!

**3D Bioprinting: Physical and Chemical Processes**

May 2–3, 2017 • Winston Salem, NC, USA

# Light- and bias-induced metastabilities in Cu(In,Ga)Se<sub>2</sub> based solar cells caused by the ( $V_{\text{Se}}-V_{\text{Cu}}$ ) vacancy complex

Stephan Lany and Alex Zunger<sup>a)</sup>

National Renewable Energy Laboratory, Golden, Colorado 80401

(Received 18 April 2006; accepted 15 September 2006; published online 13 December 2006)

We investigate theoretically light- and bias-induced metastabilities in Cu(In,Ga)Se<sub>2</sub> (CIGS) based solar cells, suggesting the Se–Cu divacancy complex ( $V_{\text{Se}}-V_{\text{Cu}}$ ) as the source of this hitherto puzzling phenomena. Due to its amphoteric nature, the ( $V_{\text{Se}}-V_{\text{Cu}}$ ) complex is able to convert by persistent carrier capture or emission from a shallow donor into a shallow acceptor configuration, and vice versa, thereby changing in a metastable fashion the local net acceptor density inside the CIGS absorber of the solar cell, e.g., a CdS/CIGS heterojunction. In order to establish a comprehensive picture of metastability caused by the ( $V_{\text{Se}}-V_{\text{Cu}}$ ) complex, we determine defect formation energies from first-principles calculations, employ numerical simulations of equilibrium defect thermodynamics, and develop a model for the transition dynamics after creation of a metastable nonequilibrium state. We find that the ( $V_{\text{Se}}-V_{\text{Cu}}$ ) complex can account for the light-induced metastabilities, i.e., the “red” and “blue” illumination effects, as well as for the reverse-bias effect. Thus, our ( $V_{\text{Se}}-V_{\text{Cu}}$ ) model implies that the different metastabilities observed in CIGS share a common origin. A defect state in the band gap caused by ( $V_{\text{Se}}-V_{\text{Cu}}$ ) in the acceptor configuration creates a potentially detrimental recombination center and may contribute to the saturation of the open circuit voltage in larger-gap Cu(In,Ga)Se<sub>2</sub> alloys with higher Ga content. Therefore, the presence of metastable defects should be regarded as a concern for solar cell performance. © 2006 American Institute of Physics. [DOI: [10.1063/1.2388256](https://doi.org/10.1063/1.2388256)]

## I. INTRODUCTION

Light-induced and voltage-bias-induced metastabilities are widely observed, yet still puzzling phenomena in Cu(In,Ga)Se<sub>2</sub> (CIGS) based solar cells.<sup>1–15</sup> The most commonly observed metastabilities are classified into three categories.<sup>7,8</sup> (i) “Red illumination,” i.e., illumination with long-wavelength light not absorbed by the window/buffer materials (ZnO/CdS), causes a metastable increase of the open circuit voltage and the capacitance of the CdS/CIGS heterojunction, due to a metastable increase of the net acceptor concentration in the CIGS absorber.<sup>1,3–5,8,11–14</sup> This effect results from persistent photoconductivity (PPC).<sup>3,6</sup> Similar metastable changes occur also after minority carrier (electron) injection via pulses of forward bias.<sup>2,3,13</sup> (ii) The “blue illumination” effect is caused by light that is absorbed in the CdS buffer layer, and leads to a decreased junction capacitance,<sup>8</sup> possibly indicating a decreased net acceptor density in the CIGS absorber. (iii) The application of “reverse bias” at or above room temperature leads to an increased junction capacitance,<sup>4,7,8,10,15</sup> similarly like red illumination, but the net acceptor density increases only within some interval at intermediate distance from the junction, and actually may decrease farther away from the junction after reverse-bias treatment.<sup>5,7,15</sup> Other experiments in CdS/CIGS solar cells, which have, however, so far not been linked to the above mentioned effects, revealed an amphoteric, metastable defect of unknown microscopic origin causing unusual capacitance transients.<sup>16,17</sup>

The presence of the metastable effects remains a concern for solar cell efficiency: While the increased net acceptor doping due to PPC after red illumination is generally considered a beneficial effect,<sup>1,3,4,7</sup> red illumination,<sup>11</sup> and reverse-bias treatment<sup>8,10</sup> alone can even deteriorate device performance. The performance-improving effect of light-soaking procedures employing white light relies on the beneficial effect of the blue illumination that counteracts, but not cancels, the possible detrimental effects of the red illumination and voltage bias metastabilities.<sup>4,7,8,10</sup> Thus, the apparent benign nature of metastability results only from a balance between beneficial and detrimental effects compensating each other to some extent.

The microscopic origin of the metastable effects (i)–(iii) outlined above has been subjected to wide speculation in the past: Metastable defects that trap carriers by undergoing a large lattice relaxation are presently to most plausible explanation for PPC.<sup>9</sup> Defects that have been proposed to cause metastability include the In<sub>Cu</sub> antisite,<sup>2</sup> interstitial Cu<sub>i</sub>,<sup>5</sup> the Se vacancy  $V_{\text{Se}}$ ,<sup>10</sup> and the Se–Cu divacancy complex  $V_{\text{Se}}-V_{\text{Cu}}$ .<sup>7</sup> In contrast to the lattice relaxation model for the red illumination effect, reversible long-range Cu migration was invoked to explain the metastable changes in the dopant profile after reverse-bias treatment.<sup>4,5</sup> Indeed, electromigration of Cu in the presence of an electric field has been directly proven by means of radiotracer methods,<sup>18</sup> where, however, much stronger electric fields have been applied than those typically present during reverse-bias treatment.

Using first-principles total-energy calculations, we recently found<sup>19,20</sup> that the anion vacancy in II–VI semiconductors and in chalcopyrite CuInSe<sub>2</sub> (CIS) and CuGaSe<sub>2</sub> (CGS)

<sup>a)</sup>Electronic mail: alex\_zunger@nrel.gov

exhibits metastable behavior that can lead to persistent photoconductivity. In Ref. 20 we discussed in detail the general defect physics that leads to metastability and PPC of anion vacancies in II-VI and chalcopyrite Cu-III-Se<sub>2</sub> compounds. We further gave in Ref. 20 preliminary results for the formation of a  $(V_{\text{Se}}-V_{\text{Cu}})$  complex of a Se vacancy with a Cu vacancy in CIS, indicating that such complexes cause metastable behavior in actual devices, rather than the isolated  $V_{\text{Se}}$ .<sup>20</sup> The purpose of the present work is to give a comprehensive account of the calculated properties of the  $(V_{\text{Se}}-V_{\text{Cu}})$  complex both in CIS and in CGS, to establish models for the dynamics (i.e., transition rates) and thermodynamics of the metastability caused by  $(V_{\text{Se}}-V_{\text{Cu}})$ , and to put the theoretical results into relation with experimental evidence of metastability.

*Précis.* We employ total-energy calculations for the  $(V_{\text{Se}}-V_{\text{Cu}})$  complex in CIS and CGS to determine defect formation energies, binding energies for the  $(V_{\text{Se}}-V_{\text{Cu}})$  complex formation, thermodynamic (equilibrium) transition levels, optical excitation and photoluminescence (PL) energies, and energy barriers in the configuration coordinate diagram (CCD). We find that the  $(V_{\text{Se}}-V_{\text{Cu}})$  complex can exist in two distinct *structural* configurations, i.e., in an acceptor and a donor configuration, which are separated by energy barriers associated with structural reconfiguration. (i) In pure CIS and low Ga content CIGS, the donor configuration produces a shallow *n*-conductive donor level (charge states 0 and 1+). In pure CGS and high Ga content CIGS, the donor configuration produces only a compensating donor state (charge state 1+). (ii) The acceptor configuration produces for all CIGS compositions a shallow *p*-conductive acceptor level (charge states 0 and 1−), similarly like the isolated  $V_{\text{Cu}}$ , but also very deep 2− and 3− acceptor states about 1 eV above the valence band maximum (VBM).

The calculated  $(+/-)$  transition between the donor and the acceptor configuration occurs at a Fermi level between about 0.2 and 0.3 eV above the VBM—depending on the CIGS alloy composition—and the transition requires the thermal activation of an energy barrier plus *simultaneous* capture of electrons (donor-to-acceptor conversion) or holes (acceptor-to-donor conversion). Upon creation of excess carriers of one type, e.g., by illumination, the equilibrium distribution between the donor and acceptor configurations is changed. The transition of the  $(V_{\text{Se}}-V_{\text{Cu}})$  complex from the donor into the acceptor configuration after persistent capture of photoexcited electrons during red illumination accounts for persistent photoconductivity, and *increases* the net acceptor concentration and the junction capacitance. Conversely, the transition from the acceptor into the donor configuration after persistent capture of holes, originally photoexcited in the CdS buffer by blue illumination, *decreases* the net acceptor concentration and the junction capacitance.

A redistribution between the donor and acceptor configurations of the  $(V_{\text{Se}}-V_{\text{Cu}})$  complex can also be achieved when the local electron and hole densities are changed by reverse bias: We distinguish three different ranges within the CIGS absorber at different distances from the heterojunction: Close to the junction, where the complex exists in the  $(V_{\text{Se}}-V_{\text{Cu}})^-$  acceptor configuration (or in the higher negative

charge states) in the relaxed state at zero bias, no configuration change is expected after reverse-bias treatment. In an intermediate range, the complex exists in the  $(V_{\text{Se}}-V_{\text{Cu}})^+$  donor configuration before and converts towards the acceptor configuration by electron capture or hole emission after reverse-bias treatment. Thus, the net acceptor density is increased in this range due to the reverse bias, leading to an increased junction capacitance. Even farther away from the junction, where essentially bulk like *p*-type conditions exist under zero bias, the net acceptor density may be decreased upon reverse bias due to the acceptor-to-donor conversion, proposed that a fraction of the  $(V_{\text{Se}}-V_{\text{Cu}})$  complexes existed before in the acceptor configuration under zero bias, which should be the case at elevated temperature, according to our thermodynamic modeling. Thus, the  $(V_{\text{Se}}-V_{\text{Cu}})$  model can account for both light- and bias-induced metastabilities, without any need to assume reversible long-range migration of atoms. At the same time, our model implies that the different metastabilities observed in CIGS share a common origin.

While the  $\varepsilon(+/-)$  transition, which corresponds to the conversion between the donor and acceptor configurations, can appear as a deep level in capacitance experiments, we emphasize that it actually results from an activated transition from a shallow donor into a shallow acceptor configuration (or vice versa) and behaves quite different than “conventional” deep levels: While conventional deep levels have usually a Stokes-shifted optical level close to the thermal transition energy, the activated  $(+/-)$  transition does not produce any optical level inside the gap. Secondly, due to the requirement of thermal activation of barriers plus the simultaneous capture of carriers, the dynamics of this transition is quite different from that of a conventional deep level, so that the conventional analysis for deep levels fails. Taking into account the thermal activation of the barrier plus the probability of carrier capture, we present a model for the capture dynamics that yields good agreement with the experimentally observed time scale for the annealing of the metastable state. Further, the dynamic model can account for a large deviation from expected frequency prefactors (i.e., the attempt frequency), as recently observed for two distinct transitions showing unusual capacitance transients.<sup>16,17</sup> Thus, the concept of a transition which requires simultaneous barrier activation plus carrier capture (or emission) may provide a physical model for the entropy factor  $\exp(\Delta S/k)$  which has been postulated in Refs. 16 and 17 as an abstract quantity that alters the effective attempt frequency.

In contrast to the activated  $\varepsilon(+/-)$  transition, the deep  $\varepsilon(-/2-)$  and  $\varepsilon(2-/3-)$  acceptor levels of  $(V_{\text{Se}}-V_{\text{Cu}})$  in the upper part of the gap are not associated by energy barriers and behave like conventional deep levels. However, these levels are present only in the acceptor configuration of the  $(V_{\text{Se}}-V_{\text{Cu}})$  complex. As long as the complex remains in the donor configuration and the energy barriers in the configuration coordinate diagram are not activated, these deep levels are absent. Like conventional deep levels, these deep acceptor levels produce optical absorption and photoluminescence levels, which, again, are only present in the acceptor configuration. Thus, we suggest that the  $(V_{\text{Se}}-V_{\text{Cu}})$  defect is the origin of recently observed optical absorption levels,<sup>21–23</sup> in-

dicating that metastable behavior of CIGS solar cells is accompanied by a potentially detrimental recombination center.

## II. METHODS

We determine the defect formation energies  $\Delta H_{D,q}$  for  $D = V_{\text{Se}}, V_{\text{Cu}}, V_{\text{Se}} - V_{\text{Cu}}$ , from total-energy supercell (64 atoms) calculations within the local density approximation (LDA) of density functional theory, employing the pseudopotential-momentum space formalism.<sup>24</sup> We use the Ceperly-Alder LDA exchange-correlation potential<sup>25</sup> as parametrized by Perdew and Zunger<sup>26</sup> and the projector augmented wave (PAW) potentials as implemented in the VASP code.<sup>27</sup> Using the calculated total energies, we obtain  $\Delta H_{D,q}$  as

$$\Delta H_{D,q}(E_F, \mu) = (E_{D,q} - E_H) + \sum \mu_\alpha + qE_F, \quad (1)$$

where the first term is the energy difference between the supercell with defect in charge state  $q$  ( $E_{D,q}$ ) and the pure host ( $E_H$ ). In the present work, we evaluate the supercell energies at the experimental lattice constant.<sup>28</sup> The second and third terms describe the energy of the atomic and electronic reservoirs, respectively. Here, the chemical potential  $\mu_\alpha$  is given with respect to the elemental phase,  $\mu_\alpha = \mu_\alpha^{\text{elem}} + \Delta\mu_\alpha$  ( $\alpha = \text{Se}, \text{Cu}$ ), and the Fermi energy  $E_F$  with respect to the VBM,  $E_F = E_v + \Delta E_F$ . From  $\Delta H$ , we also calculate the defect transition energy  $\varepsilon(q/q')$  between two charge states  $q$  and  $q'$ , i.e., the value of  $E_F$  where  $\Delta H(q, E_F) = \Delta H(q', E_F)$ . Optical (vertical) transition energies are calculated from total-energy differences as described in Ref. 20 by fixing the atomic coordinates of the initial state, according to the Franck-Condon principle. Further, we use the thermodynamic model described in Refs. 29 and 30, in which the equilibrium Fermi level is determined for a given temperature numerically by taking into account the charged defect concentrations and carrier densities subject to the charge neutrality condition.

While the general method of total-energy supercell calculations for defects in semiconductors is well established,<sup>31</sup> we emphasize here that rather large corrections with individual contributions up to few eV have to be applied to LDA supercell energies, in order to obtain accurate defect formation energies. In a recent publication<sup>32</sup> we provided technical details for the required of total-energy corrections. Since these corrections depend on whether a defect is shallow or deep (the distinction between shallow and deep defects in supercell calculations is discussed in detail in Ref. 20), it is sometimes necessary to make *a posteriori* assumptions towards the shallow or deep nature of a defect. After applying the corrections, the transition levels of shallow single donors and shallow single acceptors generally agree with the experimentally known effective-mass binding energy within 0.1 eV. Somewhat larger uncertainties, in the order of 0.2–0.3 eV, have to be expected for transition levels of multiply charged or deep defects. We now briefly review the corrections<sup>32</sup> and quantify their contributions in CIGS.

(i) *LDA band gap correction.* While the experimental band gaps of CIS and CGS are 1.04 and 1.68 eV, respectively, the LDA band gaps are  $E_g = -0.40$  eV in CIS (i.e., valence and conduction bands are overlapping by 0.40 eV)

and only 0.03 eV in CGS. In order to account for the discrepancy, we correct both the energy of the VBM,  $E_v$ , and that of the conduction band minimum (CBM). The VBM correction  $\Delta E_v = -0.37$  eV for CIS and CGS was determined<sup>20</sup> from LDA+U (Ref. 33) calculations which correct for spurious self-interaction in the Cu  $d$  orbitals. Using a similar procedure for ZnO, where LDA+U for the Zn  $d$  shell leads to  $\Delta E_v = -0.77$  eV, we found that the lowering of the VBM due to the reduced  $p$ - $d$  repulsion in LDA+U is comparable with GW calculations.<sup>34</sup> The remaining discrepancy with the experimental gap after the correction of the VBM is corrected in the conduction band, i.e.,  $\Delta E_c = 1.07$  and  $\Delta E_c = 1.28$  eV in CIS and CGS, respectively. Note that the defect formation energy  $\Delta H$  of a defect in charge state  $q$  changes by  $q\Delta E_v$  at  $E_F = E_v$ , and by  $q\Delta E_c$  at  $E_F = E_c$ , compared to  $\Delta H$  for a Fermi level at the respective uncorrected band edge energies.

(ii) *LDA correction for shallow donors/acceptors.* Shallow defects do not introduce defect-localized states (DLS) inside the band gap, even though such DLS are usually present as resonances inside the host conduction or valence bands.<sup>20</sup> Therefore, the introduced carriers (i.e., electrons/holes in case of donors/acceptors) relax to the respective band edge, where they occupy a perturbed host state (PHS),<sup>20</sup> i.e., the effective-mass-like state that is created due to the screened Coulomb potential of the charged donor (acceptor). Since such hydrogenic PHS are essentially formed by the states of the host band edges, i.e., the CBM or the VBM, it can be assumed that the full LDA correction of the host band edges applies to these states as well. For  $z_e$  ( $z_h$ ) being the number of electrons (holes) occupying a PHS in a particular charge state of a donor (acceptor), a correction of  $z_e\Delta E_c$  ( $-z_h\Delta E_v$ ) applies to  $\Delta H$ . For example,  $z_e = 2$  for the shallow neutral double donor  $\text{In}_{\text{Cu}}^0$  (Ref. 32) and  $z_h = 1$  for the shallow neutral single acceptor  $\text{V}_{\text{Cu}}^0$ .

Deep defects introduce defect-localized states inside the band gap. Since such DLS have a very different character than the delocalized host states of the CBM and the VBM, it can generally not be assumed that the LDA correction of the band edges applies to a DLS. In fact, if we do not apply any correction to the DLS that anion vacancies produce in the band gap of II-VI compounds, we obtain good agreement with experimental  $F^+$ -center absorption energies of  $V_{\text{Se}}$ ,  $V_{\text{S}}$ , and  $V_{\text{O}}$  in ZnSe, ZnS, and ZnO, respectively.<sup>19,20</sup> While DLS are generally less affected by the LDA error compared to the band edge energies (the CBM, in particular), beyond LDA methods such as the GW approximation<sup>34,35</sup> or self-interaction correction<sup>26</sup> (SIC) are required to obtain an estimate how the energy of a DLS has to be corrected. Note that neither GW nor SIC are presently total-energy methods that can reliably be applied to large-scale impurity systems. Therefore, such methods can, at best, give a hint how the LDA total-energy should be corrected, but can presently not replace the LDA total-energy calculation.

(iii) *Band filling correction for shallow donors/acceptors.* Supercell calculations of shallow defects generally imply very high, degenerate doping densities far beyond the insulator-metal transition. Since one is usually interested in the defect formation energy for a nondegenerate system, it



is needed to correct for the band-filling effects (Moss-Burstein shift) resulting from the high defect density of the actual calculation. Due to the small effective electron mass in CIS and CGS,  $m_e^*/m_e=0.09$  (Ref. 36), these band-filling effects are most strongly pronounced for donors. Thus, the respective correction for  $\Delta H$  of the intrinsic  $\text{In}_{\text{Cu}}^0$  double donor in CIS is as large as  $-1.5$  eV. Due to the larger effective hole mass,  $m_h^*/m_e=0.8$  (Refs. 37 and 38) in CIS, the band-filling correction for the single-acceptor states of  $V_{\text{Cu}}^0$  and of the  $(V_{\text{Se}}-V_{\text{Cu}})^0$  complex (in the acceptor configuration) is only about  $-0.1$  eV. Note that these band-filling effects originate from the use of finite-size supercells and not from deficiencies of the LDA.

(iv) *Potential alignment correction for charged impurities.* The supercell formalism describes a periodic, infinite system without any surface, implying that, e.g., the change of the electrostatic potential due to the surface dipole is neglected. Still, the total energy per unit cell is well defined if such a periodic system is charge neutral.<sup>24</sup> If the unit cell contains a net charge, however, the total energy diverges. For the calculation of charged systems, such as ionized donors/acceptors, this problem is usually circumvented by excluding the (diverging) constant part of the electrostatic potential, i.e., the  $\mathbf{G}=0$  term in the Fourier expansion, from the total-energy expression. However, the charged-defect formation energy obtained by this procedure now depends on the unknown offset between the average potential of the pure host system and average potential of the charged host+defect system.<sup>32</sup> We determine this potential offset  $\Delta V$  by the difference of the atomic-sphere-averaged electrostatic potentials around host atoms farther away from the defect, relative to the atomic-sphere-averaged potentials around the respective host atoms in the pure host.<sup>39</sup> For a defect in charge state  $q$ , the potential alignment correction to  $\Delta H$  is  $q\Delta V$ . In the 64 atom supercell, we obtain for the  $(V_{\text{Se}}-V_{\text{Cu}})$  complex  $\Delta V \approx -0.2$  eV both in CIS and in CGS, so that energy corrections up to  $+0.6$  eV for  $q=-3$  result from the potential alignment correction.

(v) *Image charge correction for charged defects.* The exclusion of the  $\mathbf{G}=0$  terms from the total-energy expression in the case of a charged system implies the presence of a compensating uniform background charge that restores overall charge neutrality. The effective (i.e., screened) Madelung energy of the defect charge in the jellium background is corrected to  $O(L^{-5})$ , according to Ref. 40. The image charge correction is proportional to  $q^2$ , resulting in large corrections of up to 0.85 eV in the case of the  $q=-3$  state of the  $(V_{\text{Se}}-V_{\text{Cu}})$  complex in CGS. For high charge states like  $q=-3$ , and also for shallow levels where the defect charge is not strictly localized within the supercell volume, the image charge correction possibly leads to an overcorrection.<sup>32,41</sup> Therefore, we give below all transition energies both with and without the image charge correction.

### III. AMPHOTERIC BEHAVIOR OF THE $(V_{\text{Se}}-V_{\text{Cu}})$ COMPLEX

*Electronic states of the isolated vacancies  $V_{\text{Se}}$  and  $V_{\text{Cu}}$ .* As a prerequisite for the discussion of the  $(V_{\text{Se}}-V_{\text{Cu}})$  com-

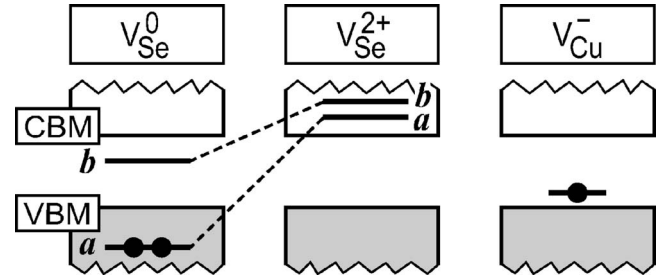


FIG. 1. Schematic energy level diagrams for the isolated Se and Cu vacancies  $V_{\text{Se}}$  and  $V_{\text{Cu}}$  in CIS.  $V_{\text{Se}}$  introduces the defect-localized states  $a$  and  $b$ , whose single-particle energies depend strongly on the In-In distance ( $d_{\text{In-In}}=3.04$  Å for  $V_{\text{Se}}^0$  and 5.45 Å for  $V_{\text{Se}}^{2+}$ ).  $V_{\text{Cu}}$  introduces a delocalized perturbed-host-state close above the VBM.

plex, we briefly review the properties of the isolated Se vacancy<sup>19,20</sup> and Cu vacancy.<sup>31,32,42</sup> The isolated Se vacancy  $V_{\text{Se}}$  in CIS and CGS introduces two defect-localized states (DLS, cf. Sec. II) in the band gap region, as shown schematically in Fig. 1: e.g., in CIS, the state denoted  $a$  results from the *bonding* In-In state formed by the symmetric combination of the two In dangling bonds, while state  $b$  is the respective *antibonding* In-In state (the labels  $a$  and  $b$  refer to the respective symmetry representations for the  $C_2$  point group of the anion vacancy in the chalcopyrite lattice). Both DLS are strongly localized at the In atoms around the vacancy, and the respective Cu dangling bond states are much higher in energy. The mechanism of anion vacancy metastability in II-VI and Cu-III-VI<sub>2</sub> compounds crucially relies on the drastic changes in atomic and electronic structures upon population and depopulation of the symmetric state formed by the cation dangling bonds,<sup>19,20</sup> i.e., the  $a$  level depicted in Fig. 1 for chalcopyrite CIS and CGS: In the neutral  $V_{\text{Se}}^0$  state where the  $a$  level is populated ( $a^2b^0$ ), a short bond between the group-III atoms around  $V_{\text{Se}}$  is formed. In this configuration, the  $a$  level is  $\sim 2$  eV deep below the VBM, while the  $b$  level lies within the upper part of the band gap (see Fig. 1). In the ionized  $V_{\text{Se}}^{2+}$  state where the  $a$  level is depopulated ( $a^0b^0$ ), the bond between the group-III atoms breaks up, leading to a large distance between the group-III neighbors of  $V_{\text{Se}}$ . At the same time, the  $a$  and  $b$  levels move towards higher energies, above the CBM of CIS (Fig. 1). We emphasize here that the large lattice relaxation (III-III bond formation/breakup), which is responsible for the metastable effects, is controlled by the *occupation* of the defect-localized  $a$  level. The calculated In-In and Ga-Ga equilibrium distances and the respective single-particle energies of the  $a$  and  $b$  levels are listed in Table I. In contrast to the *localized* defect levels of  $V_{\text{Se}}$ , i.e., the  $a$  and  $b$  DLS, the isolated Cu vacancy  $V_{\text{Cu}}^-$  introduces—due to its negative charge—a *delocalized* perturbed-host state (PHS, cf. Sec. II) just above the VBM, as shown schematically in Fig. 1, i.e.,  $V_{\text{Cu}}$  produces a shallow acceptor level.

Figure 2(a) shows as a function of the Fermi level the formation energies  $\Delta H$  of  $V_{\text{Se}}$ ,  $V_{\text{Cu}}$ , and  $V_{\text{Se}}-V_{\text{Cu}}$  in CIS (Fig. 2(a), left) and CGS (Fig. 2(a), right), along with the thermodynamic (equilibrium) transition levels. All transition energies are also listed in Table II. Since the main effect of alloying Ga into CIS is to raise the energy of the conduction

TABLE I. For the isolated  $V_{\text{Se}}$  and the  $(V_{\text{Se}}-V_{\text{Cu}})$  complex in CIS and CGS, the table gives the calculated equilibrium distances between the group-III neighbors to  $V_{\text{Se}}$ , and the corresponding single-particle energies of the  $a$  and  $b$  levels [cf. Figs. 1, 3(a), and 4(a)] with respect to the VBM.

	CIS ( $E_C=E_V+1.04$ eV)			CGS ( $E_C=E_V+1.68$ eV)		
	$d_{\text{In-In}}$ (Å)	$\varepsilon(a)$ (eV)	$\varepsilon(b)$ (eV)	$d_{\text{Ga-Ga}}$ (Å)	$\varepsilon(a)$ (eV)	$\varepsilon(b)$ (eV)
$V_{\text{Se}}^0$	3.04	-2.1	+0.9	2.83	-2.2	+0.9
$V_{\text{Se}}^{2+}$	5.45	+1.9	+2.2	5.29	+1.8	+2.2
$(V_{\text{Se}}-V_{\text{Cu}})^-$	3.05	-2.0	+1.0	2.84	-2.2	+0.9
$(V_{\text{Se}}-V_{\text{Cu}})^+$	5.43	+1.9	+2.2	5.23	+1.6	+2.0

band minimum,<sup>42</sup> the range of possible Fermi levels in Fig. 2(a) (left) is extended above the CBM of pure CIS, up to  $E_F=E_V+1.25$  eV, approximately corresponding to the CBM of  $\text{CuIn}_{1-x}\text{Ga}_x\text{Se}_2$  alloys with compositions up to  $x \leq 0.4$ , as used for high efficiency CIGS solar cells. We see in Fig. 2(a) (left) that in CIS, the isolated  $V_{\text{Se}}$  has a deep, negative- $U$ -like, double donor transition  $\varepsilon(2+/0)=E_V+0.05$  eV close to the VBM, and deep acceptor transitions high in the gap, i.e.,  $\varepsilon(0/-)=E_V+0.85$  eV and  $\varepsilon(-/2-)=E_V+1.14$  eV.<sup>39</sup> These deep acceptor levels result from the occupation of the antibonding  $b$  level (Fig. 1), leading to the formations of  $V_{\text{Se}}^-$  ( $a^2b^1$ ) and  $V_{\text{Se}}^{2-}$  ( $a^2b^2$ ). Thus, the isolated  $V_{\text{Se}}$  exhibits amphoteric behavior having both deep donor and deep acceptor levels, where the usual order of the donor and acceptor levels is inverted, i.e., the acceptor transitions occur higher in the gap than the donor transition. Notably, we find very similar transition energies (measured with respect to the VBM) for  $V_{\text{Se}}$  in CGS, shown in Fig. 2(a) (right), despite the higher energy of the CBM in CGS. The isolated Cu vacancy  $V_{\text{Cu}}$  has

a shallow acceptor transition close to the VBM both in CIS and in CGS (Fig. 2(a)). Because of this shallow acceptor level and the low formation energy, even under maximally Cu-rich conditions ( $\Delta\mu_{\text{Cu}}=0$ ),  $V_{\text{Cu}}$  causes net  $p$ -type doping in CIS and CGS under most growth conditions.<sup>29,30</sup>

*Thermodynamic stability of the  $(V_{\text{Se}}-V_{\text{Cu}})$  vacancy complex.* Figure 2(b) shows the calculated binding energy  $E_b$  of the  $(V_{\text{Se}}-V_{\text{Cu}})$  complex, obtained from the difference of the complex formation energy and the formation energies of the isolated vacancies, i.e.,  $E_b=\Delta H(V_{\text{Se}}-V_{\text{Cu}})-\Delta H(V_{\text{Se}})-\Delta H(V_{\text{Cu}})$ . We see that for Fermi levels up to about 1 eV, the binding energy is  $-0.5$  eV or lower, indicating that  $V_{\text{Se}}$  binds  $V_{\text{Cu}}$ . Since Cu vacancies are known to be very mobile in CIS,<sup>18,43</sup> we expect that  $V_{\text{Cu}}$  will equilibrate to form the  $(V_{\text{Se}}-V_{\text{Cu}})$  complex at room temperature. From the law of mass action, i.e.,  $[(V_{\text{Se}}-V_{\text{Cu}})]=[V_{\text{Se}}][V_{\text{Cu}}]\exp(-E_b/kT)$ , we find that practically all Se vacancies will be present as complexes at  $T \approx 300$  K if the concentration of uncompensated Cu vacancies exceeds  $10^{14} \text{ cm}^{-3}$ , which is generally the case in these materials. (Since the concentration of  $V_{\text{Cu}}$  generally exceeds that of  $V_{\text{Se}}$ , unbound Cu vacancies will still exist.) Thus, for the issue of metastability in solar cell devices, one must consider the properties of the  $(V_{\text{Se}}-V_{\text{Cu}})$  vacancy complex, rather than those of the isolated  $V_{\text{Se}}$ .

*Transition energies of the  $(V_{\text{Se}}-V_{\text{Cu}})$  complex.* After the pairing of  $V_{\text{Se}}$  and  $V_{\text{Cu}}$  to form the  $(V_{\text{Se}}-V_{\text{Cu}})$  complex, the  $a$  and  $b$  defect-localized states occur at very similar energies compared to the isolated  $V_{\text{Se}}$  (Table I). Also, the equilibrium In-In (Ga-Ga) distances change little due to the pairing of  $V_{\text{Se}}$  with  $V_{\text{Cu}}$  (Table I). Thus, the basic mechanism of the metastability of  $V_{\text{Se}}$ , i.e., the III-III bond formation and breakup, along with the associated shift in the defect level energies, is still operational after pairing with  $V_{\text{Cu}}$ . Owing to

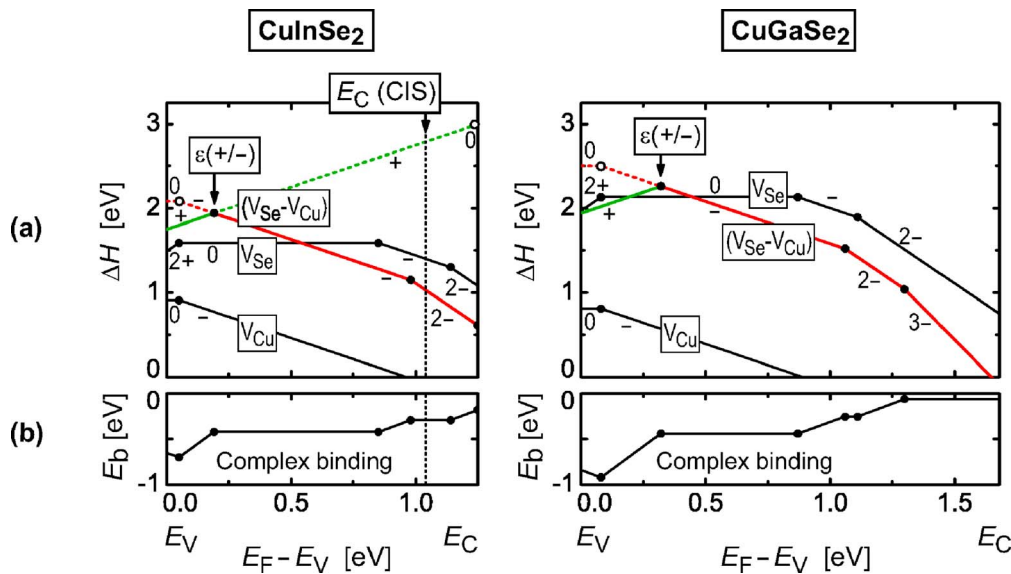


FIG. 2. (Color online) (a) Defect formation energies  $\Delta H$  of  $V_{\text{Se}}$ ,  $V_{\text{Cu}}$ , and  $(V_{\text{Se}}-V_{\text{Cu}})$  in CIS and CGS under Se-poor (CIS:  $\Delta\mu_{\text{Se}}=-0.83$  eV, CGS:  $\Delta\mu_{\text{Se}}=-0.86$  eV) and maximally Cu-rich ( $\Delta\mu_{\text{Se}}=0$ ) growth conditions, (Ref. 30), as a function of the Fermi level  $E_F$  (the values including the image charge correction from Sec. II are used here, cf. Table I). The range of  $E_F$  in CIS is extended above the CBM of pure CIS, in order to illustrate the situation in larger-gap CIGS alloys. The solid circles mark the equilibrium transition energies  $\varepsilon(q/q')$  (cf. Table II). The dashed lines indicate the metastable character of  $(V_{\text{Se}}-V_{\text{Cu}})$  in the donor configuration (green, large In-In distance) when  $E_F > \varepsilon(+/-)$ , and of  $(V_{\text{Se}}-V_{\text{Cu}})$  in the acceptor configuration (red, short In-In or Ga-Ga distance), when  $E_F < \varepsilon(+/-)$ . The open circles mark the shallow  $\varepsilon^*(0/+)$  donor and  $\varepsilon^*(0/-)$  acceptor transition energies of the metastable configurations, which are observable only under conditions where the activated  $\varepsilon(+/-)$  transition is suppressed, e.g., at low temperature. (b) Binding energy  $E_b$  of the  $(V_{\text{Se}}-V_{\text{Cu}})$  complex obtained as the difference of the  $\Delta H$  of the complex with respect to  $\Delta H$  of the isolated vacancies.

TABLE II. Calculated transition energies in eV for the  $(V_{\text{Se}}-V_{\text{Cu}})$  complex and the isolated vacancies  $V_{\text{Se}}$  and  $V_{\text{Cu}}$  in CIS and CGS [cf. Fig. 2(a)]. For the complex, the table gives the equilibrium transitions  $\varepsilon(+/-)$ ,  $\varepsilon(-/2-)$ , and  $\varepsilon(2-/3-)$ , and the shallow donor and acceptor levels that occur in a metastable configuration, i.e.,  $\varepsilon^*(0/+)$  and  $\varepsilon^*(0/-)$  (cf.  $E_d$  and  $E_a$  Figs. 3 and 5). Further, the optical absorption ( $E_{\text{abs}}$ ) and emission ( $E_{\text{PL}}$ ) energies, as well as the energy barriers  $\Delta E_1$ ,  $\Delta E_2$ , and  $\Delta E_3$  [cf. Figs. 3(b) and 5(b)], are given (Ref. 45). The values obtained when neglecting the image charge correction (cf. Sec. II) are given in parentheses. For the isolated vacancies, the table gives the equilibrium transition energies.

	CIS	CGS
$(V_{\text{Se}}-V_{\text{Cu}})$		
$\varepsilon(+/-)$	$E_V+0.19$ (+0.19)	$E_V+0.32$ (+0.32)
$\varepsilon(-/2-)$	$E_V+0.98$ (+0.76)	$E_V+1.06$ (+0.78)
$\varepsilon(2-/3-)$	$E_V+1.25$ (+0.89)	$E_V+1.30$ (+0.83)
$\varepsilon^*(0/+) (E_d)$	$E_C-0.07$ (+0.00)	—
$\varepsilon^*(0/-) (E_a)$	$E_V+0.06$ (-0.01)	$E_V+0.08$ (-0.01)
$E_{\text{abs}}(-/2-)$	1.05 (0.83)	1.19 (0.90)
$E_{\text{PL}}(2-/3-)$	0.88 (0.66)	0.92 (0.64)
$\Delta E_1$	~0.1	0
$\Delta E_2$	0.35	0.28
$\Delta E_3$	0.73	0.92
$V_{\text{Se}}$		
$\varepsilon(2+/0)$	$E_V+0.05$ (+0.19)	$E_V+0.14$ (+0.33)
$\varepsilon(0/-)$	$E_V+0.85$ (+0.76)	$E_V+0.87$ (+0.78)
$\varepsilon(-/2-)$	$E_V+1.14$ (+0.92)	$E_V+1.11$ (+0.82)
$V_{\text{Cu}}$		
$\varepsilon(0/-)$	$E_V+0.06$ (-0.01)	$E_V+0.08$ (-0.01)

the acceptor nature of  $V_{\text{Cu}}$ , however, the corresponding charge states of the  $(V_{\text{Se}}-V_{\text{Cu}})$  complex are shifted by  $-1$  relative to the isolated  $V_{\text{Se}}$ . As illustrated in Fig. 3(a) (right hand side) for CIS, the  $a$  and  $b$  levels are depopulated ( $a^0b^0$ ) in the singly charged  $(V_{\text{Se}}-V_{\text{Cu}})^+$  state having the atomic configuration with the large In-In distance. This configuration corresponds to the  $V_{\text{Se}}^{2+}$  state of the isolated Se vacancy. Due to its positive charge,  $(V_{\text{Se}}-V_{\text{Cu}})^+$  creates a perturbed-host state just below the CBM and acts as a shallow donor ( $E_d$  in Fig. 3) in this configuration. When the  $a$  level is occupied ( $a^2b^0$ ), like in case of the neutral  $V_{\text{Se}}^0$ , the complex assumes the short In-In distance configuration of  $(V_{\text{Se}}-V_{\text{Cu}})^-$  shown in Fig. 3(a) (left hand side). In this configuration,  $(V_{\text{Se}}-V_{\text{Cu}})$  acts as a shallow acceptor by binding a hole in the PHS created by the negative defect charge ( $E_a$  in Fig. 3). Note that due to a different method used for the determination potential alignment of the defected supercell with respect to the pure host (see above), we previously found in Ref. 20 a somewhat deeper acceptor state of  $(V_{\text{Se}}-V_{\text{Cu}})$ .<sup>39</sup> The present calculations indicate, however, that the acceptor state of the complex is shallow, and should be very similar to that of the isolated  $V_{\text{Cu}}$  (see Table II).

At  $E_F = \varepsilon(+/-)$ , the equilibrium stable state [solid lines in Fig. 2(a)] of  $(V_{\text{Se}}-V_{\text{Cu}})$  changes from the positively charged donor configuration [large III-III distance, green line in Fig. 2(a)] to the negatively charged acceptor configuration [short III-III distance, red lines in Fig. 2(a)]. However, due to energy barriers associated with the  $\varepsilon(+/-)$  equilibrium transition (see below), the donor configuration can exist as a

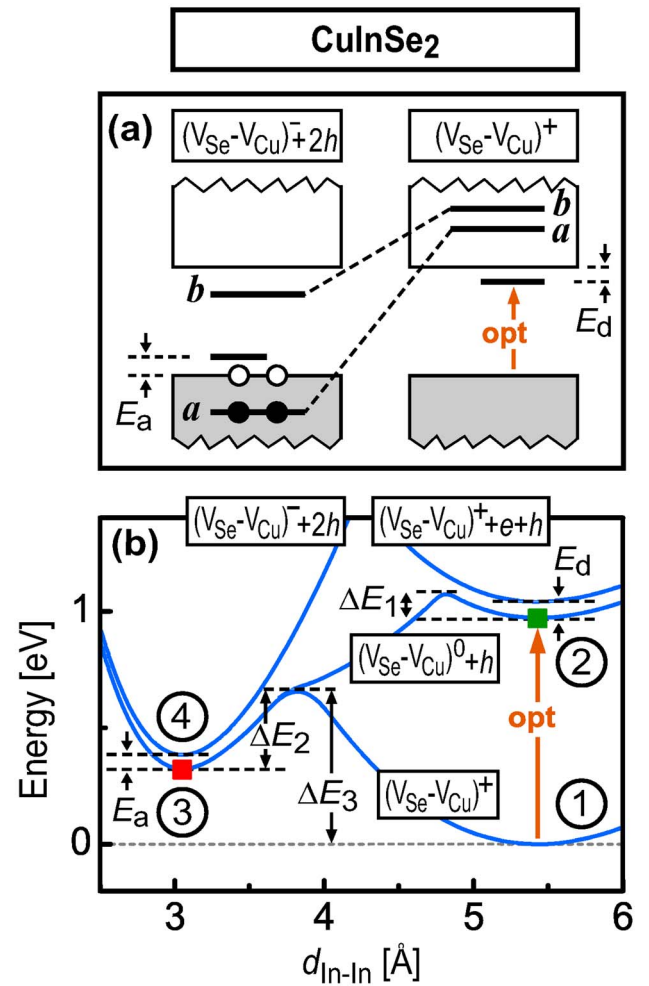


FIG. 3. (Color online) (a) Schematic energy level diagram for the  $(V_{\text{Se}}-V_{\text{Cu}})$  vacancy complex in CIS. (b) Configuration coordinate diagrams showing the energies of the different charge states of  $(V_{\text{Se}}-V_{\text{Cu}})$ , relative to  $(V_{\text{Se}}-V_{\text{Cu}})^+$ , which is the initial configuration of the optical cycle for the red illumination effect. The total charge is conserved by addition of free electrons ( $e$ ) and holes ( $h$ ). The green and red squares indicate the relaxed In-In distance of the donor and acceptor configurations of  $(V_{\text{Se}}-V_{\text{Cu}})$ , respectively. The respective relative energies correspond to  $E_F = E_V$  in Fig. 2(a).

metastable configuration for  $E_F > \varepsilon(+/-)$  in CIS and low Ga content CIGS alloys [green dashed line in Fig. 2(a), left], and the acceptor configuration can exist as a metastable configuration for  $E_F < \varepsilon(+/-)$  in CIGS of all compositions [red dashed lines in Fig. 2(a)]. The absence of a metastable donor configuration for  $E_F > \varepsilon(+/-)$  in pure CGS [Fig. 2(a), right] is due to the vanishing barrier for the conversion from the donor into the acceptor configuration in CGS (see below). Since the shallow  $\varepsilon^*(0/+)$  donor and  $\varepsilon^*(0/-)$  acceptor transitions (Table II) of the  $(V_{\text{Se}}-V_{\text{Cu}})$  complex [open circles in Fig. 2(a)] occur in metastable configurations, they are non-equilibrium transitions, which we denote by the asterisk. Still, these transitions may be observed in experiment under conditions where the energy barrier associated with the  $\varepsilon(+/-)$  transition is not activated, i.e., at lower temperature or when the change of the (quasi) Fermi level, e.g., in a capacitance experiment, occurs at higher frequency than the effective frequency of the activated  $\varepsilon(+/-)$  transition.

For CIS, the atomic structure of the  $(V_{\text{Se}}-V_{\text{Cu}})$  complex is



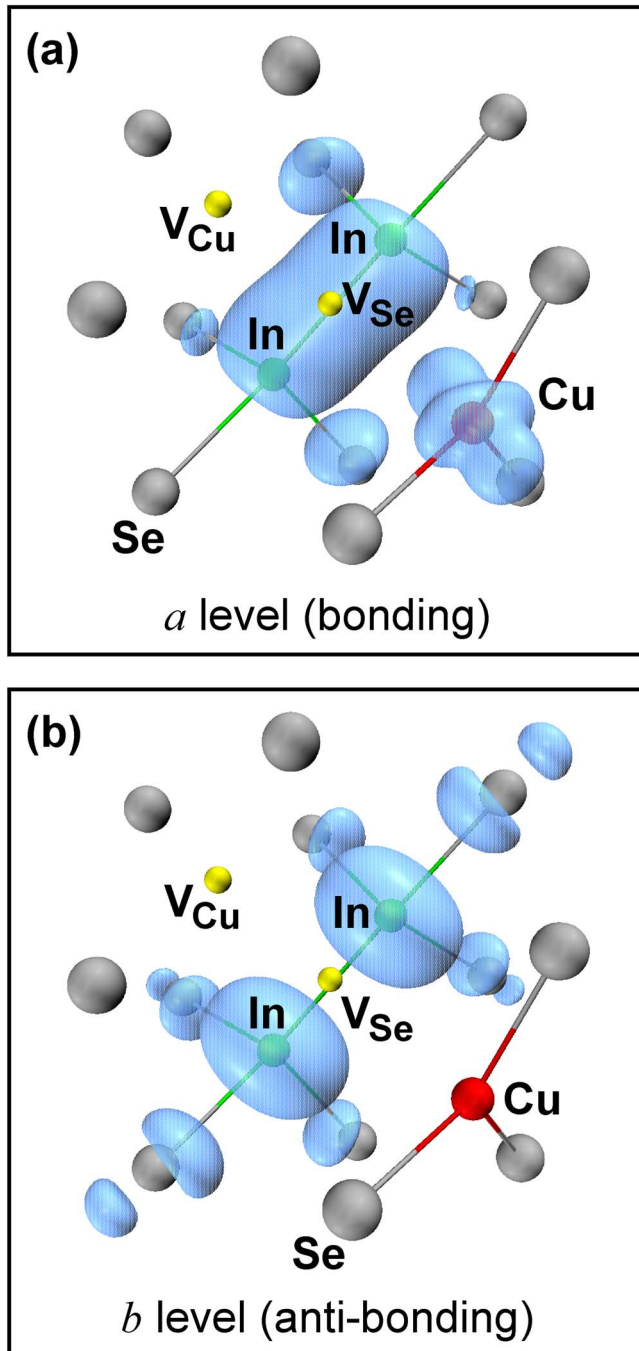


FIG. 4. (Color online) Atomic structure of the  $(V_{\text{Se}}-V_{\text{Cu}})$  complex in CIS in the acceptor configuration with the short In-In interatomic distance  $d_{\text{In-In}} = 3.05$  Å (gray: Se, green: In, red: Cu). The small spheres (yellow) mark the positions of the vacancies. Also shown are the electronic orbitals, i.e., the wave function square (blue), of (a) the  $a$  and (b) the  $b$  defect levels [cf. Fig. 3(a)], using isosurface densities of  $0.01$   $e/\text{\AA}^3$  in (a) and  $0.02$   $e/\text{\AA}^3$  in (b).

shown in Fig. 4 (Ref. 44) for the acceptor configuration with the short In-In distance, along with the electronic orbitals (isosurface plot of the wave function square) of the  $a$  and  $b$  defect levels, which, in this configuration, lie below the VBM and in the band gap, respectively (Table I). The bonding and the antibonding characters of the  $a$  and the  $b$  levels, respectively, are clearly visible in Fig. 4.

The deep  $\varepsilon(-/2-)$  and  $\varepsilon(2-/3-)$  acceptor transitions of the complex (Table II), which result from the occupation of the antibonding  $b$  level, occur at somewhat higher energy

[Fig. 2(a)] compared to the respective  $\varepsilon(0/-)$  and  $\varepsilon(-/2-)$  levels of the isolated  $V_{\text{Se}}$ . The position of the deep acceptor levels around 1 eV above the VBM indicates that in a CIGS solar cell, these levels can only be occupied very close to the CdS/CIGS heterojunction, where the Fermi level can rise to such high energies. Even though the occupation of these deep levels is accompanied by considerable atomic relaxation, no energy barriers are involved. Consequently, the deep acceptor levels are equilibrium transitions. Note, however, that these deep levels are present only in the acceptor configuration (short III-III distance), where the  $b$  level is located inside the band gap [Fig. 3(a)]. In contrast, no such deep transition levels exist as long as the complex remains in the donor configuration (large III-III distance), because the  $b$  level is outside the band gap, i.e., above the CBM, in this configuration [Fig. 3(a)].

In the acceptor-configuration of  $(V_{\text{Se}}-V_{\text{Cu}})$ , there exist also optical transitions caused by the  $b$  level in the gap: The optical absorption energies due to photoexcitation of electrons from the VBM into the  $b$  level ( $a^2b^0 \rightarrow a^2b^1 + h$ ), and the photoluminescence energies due to recombination of electrons in the  $b$  level with holes at the VBM ( $a^2b^1 + h \rightarrow a^2b^0$ ), are given in Table II. Later in Sec. V, we compare these optical energies to experimentally observed absorption and PL energies. Unlike the  $\varepsilon(-/2-)$  and  $\varepsilon(2-/3-)$  acceptor transitions which are caused by occupation of a gap state, i.e., the  $b$  level, the activated  $\varepsilon(+/-)$  transition inside the gap rather demarks the Fermi level at which the thermodynamically stable state of  $(V_{\text{Se}}-V_{\text{Cu}})$  changes from the donor to the acceptor configuration. The single-particle state being occupied during this transition, i.e., the  $a$  level, is outside the band gap before as well as after the transition [Fig. 3(a)] and, therefore, does not cause an optical transition level within the gap.

*Configuration coordinate model for the conversion between the donor and acceptor configurations.* Figure 3(b) shows the calculated configuration coordinate diagram for the  $(V_{\text{Se}}-V_{\text{Cu}})$  complex in CIS. Here, the distance  $d_{\text{In-In}}$  between the In atoms serves as the reaction coordinate. As shown in Fig. 2(a), the  $(V_{\text{Se}}-V_{\text{Cu}})^+$  state in the donor configuration with large  $d_{\text{In-In}}$  [1 in Fig. 3(b)] has the lowest energy in  $p$ -type CIGS, where the Fermi level is close to the VBM. In this configuration, the empty  $a$  level is at  $E_V + 1.9$  eV in CIS, i.e., above the CBM [see Table I and Fig. 3(a)]. In order to establish an optical cycle in the CCD, we assume that an electron-hole pair is created by photoexcitation above the CIS band gap energy [1  $\rightarrow$  2 in Fig. 3(b)]. Due to the  $a$  level energy above the CBM, the photoexcited electron does not occupy this defect-localized state, but remains in the conduction band or occupies the perturbed-host state, i.e., the delocalized shallow donor level just below the CBM ( $E_d$  in Fig. 3). After thermal activation of the energy barrier  $\Delta E_1 \approx 0.1$  eV (Ref. 45) (Table II), the  $a$  level drops below the CBM for  $d_{\text{In-In}} < 4.8$  Å, so that the electron can be captured into it ( $a^0 + e \rightarrow a^1$ ). Once the  $a$  level is occupied by one electron, atomic relaxation [2  $\rightarrow$  3 in Fig. 3(b)] leads to the acceptor configuration with the short In-In distance  $d_{\text{In-In}} = 3.05$  Å. During this relaxation, the  $a$  level drops below the VBM at  $d_{\text{In-In}} < 3.9$  Å and, therefore, captures a second elec-



tron ( $a^1 \rightarrow a^2 + h$ ), leading to a hole in the shallow acceptor level ( $E_a$  in Fig. 3), which is subsequently thermally excited into the valence band [ $3 \rightarrow 4$  in Fig. 3(b)] to form the ionized, negatively charged  $(V_{\text{Se}}-V_{\text{Cu}})^-$  state of the complex [Fig. 3(a), left hand side]. Thus, the activated (with  $\Delta E_1$ ) capture of one electron leads to the defect reaction



where the complex converts from the donor into the acceptor configuration, leading to an *increased* net acceptor concentration in the generally net *p*-type CIGS absorber.

There reverse reaction which closes the optical cycle [ $4 \rightarrow 1$  in Fig. 3(b)] requires thermal activation across  $\Delta E_2 = 0.35$  eV (Table II), plus simultaneous capture of *two* holes into the *a* level:



During this reaction, the complex converts from the acceptor into the donor configuration, leading to a *decreased* net acceptor concentration.

For both reactions (2) and (3), the transition requires an activation over an energy barrier in the CCD, plus the *simultaneous* capture of carriers. This is seen in Fig. 3(b), where a thermal activation without carrier capture, i.e., without a charge state change, leads only to oscillations around the equilibrium In-In distances 5.43 Å for  $(V_{\text{Se}}-V_{\text{Cu}})^+$  and around 3.05 Å for  $(V_{\text{Se}}-V_{\text{Cu}})^-$ . The donor/acceptor conversion according to Eqs. (2) and (3) constitutes the basic mechanism needed to explain within the  $(V_{\text{Se}}-V_{\text{Cu}})$  model the different metastable effects outlined in the Introduction (see Sec. V).

It is noted here that Eqs. (2) and (3) can occur also in the respective backward directions, which is not relevant for the optical cycle described here, but may be relevant under different conditions, e.g., reverse bias (see below). In the backward direction, Eq. (2) describes the acceptor-to-donor conversion by hole capture plus electron emission, which is associated with an energy barrier of  $\Delta E = 0.76$  eV in CIS [cf. Fig. 3(b), transition  $4 \rightarrow 2$ ]. However, due to the larger barrier, this transition is under most conditions (except for very low hole densities) slower than Eq. (3) in the forward direction (acceptor-to-donor conversion by capture of two holes) and is, therefore, not further considered. Transition, Eq. (3), in the backward direction describes the donor-to-acceptor conversion by emission of two holes, which is associated with an energy barrier of  $\Delta E_3 = 0.73$  eV in CIS [Table I, see also Fig. 3(b), transition  $1 \rightarrow 4$ ]. This transition is discussed below in the context of reverse-bias metastability. In principle, there exists a third reaction, i.e.,  $(V_{\text{Se}}-V_{\text{Cu}})^+ + 2e \leftrightarrow (V_{\text{Se}}-V_{\text{Cu}})^-$ , which is, however, not relevant: In the forward direction (donor-to-acceptor conversion by capture of two electrons) this transition is superseded by Eq. (2) which is faster because it requires capture of only one electron. In the backward direction (acceptor-to-donor conversion by emission of two electrons), this transition is associated with a very large energy barrier well above 1 eV, which inhibits this transition in the temperature range considered here (up to 400 K).

*The  $(V_{\text{Se}}-V_{\text{Cu}})$  complex in the larger-gap CGS. So far, we*

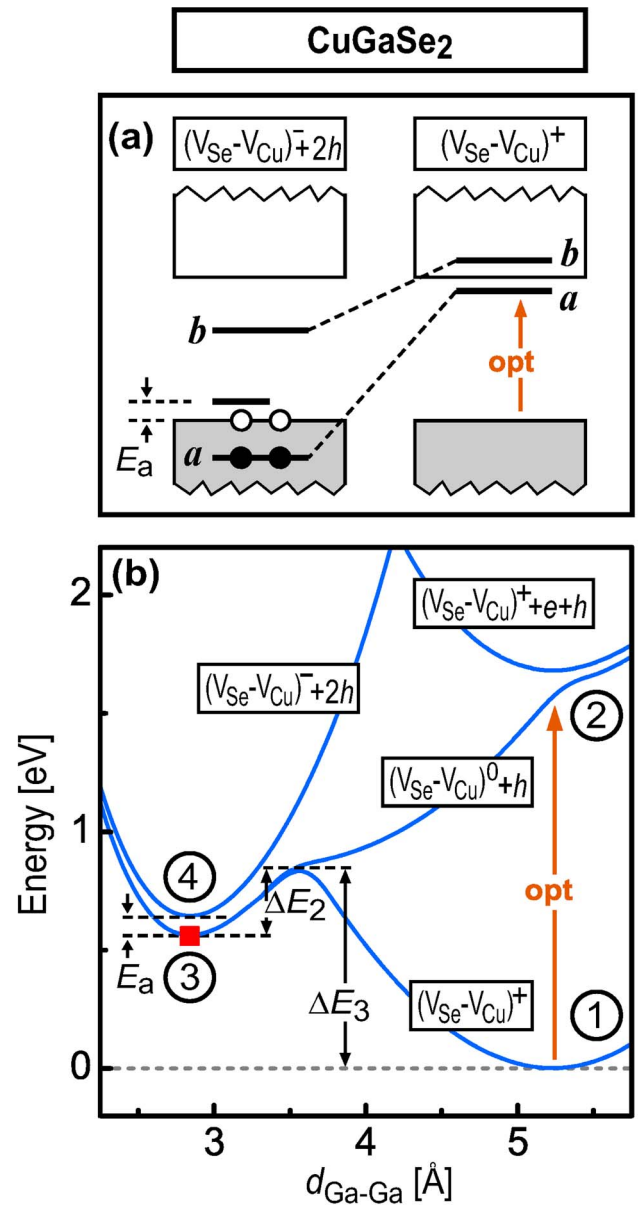


FIG. 5. (Color online) (a) Schematic energy level diagram for the  $(V_{\text{Se}}-V_{\text{Cu}})$  vacancy complex in CGS. (b) Configuration coordinate diagrams like in Fig. 3(b), but for CGS. Note that the donor configuration [green square in Fig. 3(b), CIS] does not exist in CGS, because electron capture of  $(V_{\text{Se}}-V_{\text{Cu}})^+$ , i.e., the transition  $2 \rightarrow 3$ , leads without barrier to the formation of the acceptor configuration (red square) with the short Ga-Ga distance.

discussed the  $(V_{\text{Se}}-V_{\text{Cu}})$  properties mainly for CIS and lower gap CIGS, and we now turn to the differences that occur in the larger-gap CGS. The schematic energy level diagram for CGS in Fig. 5(a) (see also Table I) shows that the *a* level is close to the CBM, but *inside* the band gap in the donor configuration  $(V_{\text{Se}}-V_{\text{Cu}})^+$ . Therefore, photoexcited or electrically injected electrons will immediately occupy this localized level, and not the delocalized perturbed-host state as in lower-gap CIGS, where the *a* level is resonant above the CBM. Since the occupation of the *a* level controls the large lattice relaxation into the acceptor configuration with short Ga-Ga distance, the immediate occupation of the *a* level implies that there is no activation barrier for the electron capture process of Eq. (2), i.e.,  $\Delta E_1 = 0$  in the configuration co-

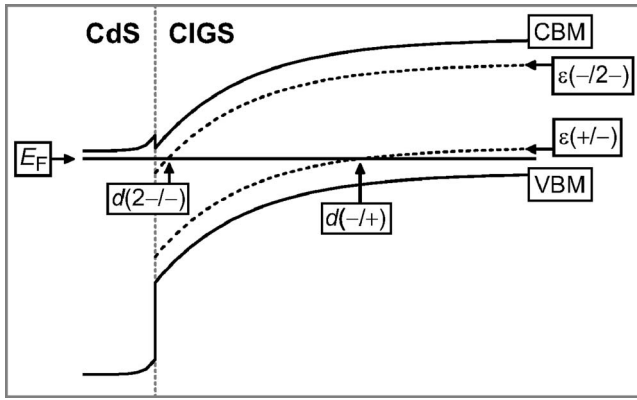


FIG. 6. Schematic band diagram of an unbiased CdS/CIGS junction shown as a function of the distance  $d$  from the junction. At  $d=d(2-/+)$ , the Fermi level intersects the  $\epsilon(-/2-)$  transition of  $(V_{Se}-V_{Cu})$ , leading to the 2- state of the complex closer to the junction. For  $d(2-/+) < d < d(-/+)$ , the complex exists in the 1- state (acceptor-configuration). For  $d > d(-/+)$ , the complex exists mainly in the 1+ state (donor-configuration), but at elevated temperature, donor and acceptor configurations may coexist. Note that  $d(-/+)$  is usually inside the space-charge region.

ordinate diagram for CGS [Fig. 5(b)]. Consequently, the  $n$ -conductive metastable donor state that exists in CIS for  $E_F > \epsilon(+/-)$  [dashed green line in Fig. 2(a), CIS] does not exist in CGS [cf. Fig. 2(a), CGS]. In CGS, once  $E_F$  rises above the  $\epsilon(+/-)$  transition level, the positively charged complex will convert via Eq. (2) into the  $(V_{Se}-V_{Cu})^-$  acceptor configuration, even at low temperature. Thus, the donor configuration with large Ga-Ga distance exists in CGS only as a *compensating* donor for  $E_F < (\epsilon(+/-))$ . In contrast, the metastable shallow acceptor state [red dashed line in Fig. 2(a)] exists in CGS similarly like in lower-gap CIS (cf.  $E_a$  in Table II). The only difference is the slightly lower energy barrier associated with the hole capture process of Eq. (3) and the somewhat larger energy barrier for hole emission by transition Eq. (3) in the backward direction, i.e.,  $\Delta E_2 = 0.28$  eV and  $\Delta E_3 = 0.92$  eV in CGS [cf. Fig. 5(b)].

#### IV. DYNAMICS AND THERMODYNAMICS OF THE DONOR/ACCEPTOR CONVERSION OF $(V_{Se}-V_{Cu})$

*Distribution between the donor/acceptor configurations of  $(V_{Se}-V_{Cu})$ , determined from the Fermi level in thermodynamic equilibrium.* In order to assess the changes in the net acceptor density upon illumination or reverse-bias treatment, we need to determine the distribution between the donor and acceptor configurations of the  $(V_{Se}-V_{Cu})$  complex before the treatment, i.e., in the relaxed state at zero bias. Since the equilibrium stable charge state of  $(V_{Se}-V_{Cu})$  depends on the local Fermi level [cf. Fig. 2(a)], it will change as a function of distance  $d$  from the CdS/CIGS heterojunction in a solar cell, as shown schematically in Fig. 6: Very close to the junction, i.e., for  $d < d(2-/+)$  in Fig. 6, where the Fermi level is very high in the gap, the complex will form the 2- state. For  $d(2-/+) < d < d(-/+)$ , the complex will exist as  $(V_{Se}-V_{Cu})^-$  in the shallow acceptor configuration. Farther away from the junction at  $d > d(-/+)$ , where the Fermi level is below the  $\epsilon(+/-)$  transition level [cf. Figs. 6 and 2(a)], the complex will exist as a compensating donor in the

$(V_{Se}-V_{Cu})^+$  state. At elevated temperature, however,  $E_F$  may approach or exceed the  $\epsilon(+/-)$  transition level, even deep inside the absorber where essentially bulklike  $p$ -type conditions exist, so that the complex may still partly exist in the  $(V_{Se}-V_{Cu})^-$  acceptor configuration at large distances from the junction.

More quantitatively, we apply the formalism for defect thermodynamics of Ref. 29 to calculate the equilibrium  $E_F$  as a function of temperature in bulklike, net  $p$ -type  $\text{CuIn}_{1-x}\text{Ga}_x\text{Se}_2$ , representing the situation in a CdS/CIGS cell far from the junction. Here, we assume an alloy composition  $x=0.3$  for which the band gap is about 1.2 eV. For simplicity, we take the weighted average  $\epsilon(+/-) = E_V + 0.23$  eV between CIS and CGS for the  $\epsilon(+/-)$  equilibrium transition (cf. Table II). Further, we use effective electron and hole masses for CIS, i.e.,  $m_h^*/m_e = 0.09$  (Ref. 36) and  $m_h^*/m_e = 0.8$ .<sup>37,38</sup> The persistent photoconductivity effect typically accounts for an increase in the net acceptor doping from the  $10^{15}$  to the  $10^{16}$   $\text{cm}^{-3}$  range.<sup>5,9,11-14</sup> Identifying this change with the conversion of the  $(V_{Se}-V_{Cu})$  complex from the (compensating) donor into the acceptor configuration (see below), we model this situation by choosing  $c(V_{Cu}) = 1.5 \times 10^{16} \text{ cm}^{-3}$  and  $c(V_{Se}-V_{Cu}) = 1.0 \times 10^{15} \text{ cm}^{-3}$ . With these values, the net acceptor density changes by a factor of 5 from  $5 \times 10^{15}$  to  $2.5 \times 10^{16} \text{ cm}^{-3}$  when all  $(V_{Se}-V_{Cu})$  complexes are converted from the compensating donor into the acceptor configuration. Note that  $c(V_{Cu})$  represents here the concentration of Cu vacancies that are not compensated by other donors such as  $\text{In}_{\text{Cu}}^{2+}$ ; the actual density of  $V_{Cu}$  may be larger due to the presence of such other donors.

Figures 7(a) and 7(b) show the calculated equilibrium Fermi level and the concentrations of the donor and acceptor configurations of  $(V_{Se}-V_{Cu})$ , respectively, as a function of temperature  $T$ . At low temperature, the complex exists mostly as  $(V_{Se}-V_{Cu})^+$ . As  $E_F$  increases with temperature, more complexes convert to  $(V_{Se}-V_{Cu})^-$ , thereby counteracting the increase of the Fermi energy, leading to modest Fermi level pinning at the  $\epsilon(+/-)$  level around room temperature. Once most complexes converted to the acceptor configuration above  $T=340$  K, the Fermi level is depinned and rises again faster with temperature. The pinning of  $E_F$  due to the amphoteric nature of  $(V_{Se}-V_{Cu})$  leads to a S-like shape the graph in Fig. 7(a), which is modestly pronounced in the present example, but could be much stronger for larger concentrations of  $(V_{Se}-V_{Cu})$ . We conclude from the results shown in Fig. 7 that below room temperature, the complex exists almost exclusively in the compensating donor configuration  $(V_{Se}-V_{Cu})^+$  deeper in the absorber, where bulklike,  $p$ -type conditions exist. Around  $T=340$  K, the acceptor configuration becomes the dominant configuration, but both configurations coexist in some temperature interval  $300 \text{ K} \leq T \leq 370 \text{ K}$ , due to the above described pinning behavior (the temperature ranges given here may change somewhat if the defect concentrations deviate from the present example). The pinning behavior of  $(V_{Se}-V_{Cu})$  further implies that the two configurations coexist over some range around the distance  $d=d(-/+)$  from the heterojunction (cf. Fig. 6), i.e., where the Fermi level approaches the  $\epsilon(+/-)$  equilibrium transition level.

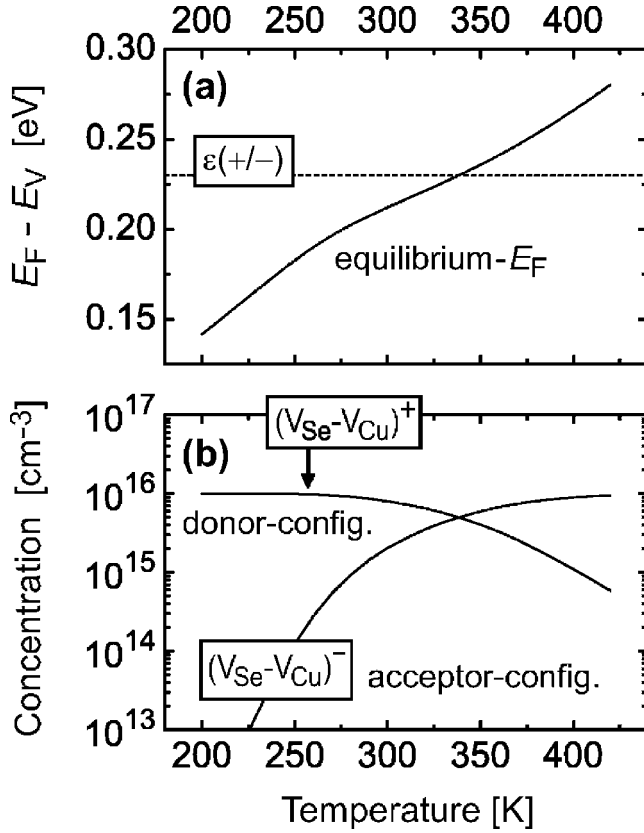


FIG. 7. (a) The equilibrium Fermi level calculated as a function of temperature, assuming concentrations of  $1.5 \times 10^{16} \text{ cm}^{-3}$  uncompensated  $V_{Cu}$  acceptors, plus  $1.0 \times 10^{16} \text{ cm}^{-3}$  amphoteric  $(V_{Se}-V_{Cu})$  complexes. (b) The corresponding equilibrium distribution between the donor and the acceptor configuration of  $(V_{Se}-V_{Cu})$ , as a function of temperature.

**Dynamics of donor/acceptor conversion.** The equilibrium distribution between the donor and the acceptor configuration should be regarded as a steady state situation with respect to the forward and backward directions of the transitions Eqs. (2) and (3). We now address the transition dynamics, i.e., the transition rates of Eqs. (2) and (3), with which a new equilibrium between the donor and acceptor configurations of  $(V_{Se}-V_{Cu})$  is established, once an external perturbation is applied, e.g., illumination or bias. If the external perturbation creates an excess of free electrons, the complex will react to this perturbation by the electron capture, Eq. (2) in the forward direction, and the conversion into the acceptor state, thereby reducing the electron excess according to Le Chatelier's principle. Similarly, if the external perturbation creates an excess of free holes, the complex will react by the hole capture, Eq. (3) in the forward direction, and the conversion into the donor state, thereby reducing the hole density. If the external perturbation creates a deficit of holes, the complex can react by the hole emission, Eq. (3) in the backward direction, and the conversion into the acceptor state, thereby increasing the hole density. In particular, around the distance  $d=d(-/+)$  (Fig. 6) where the two configurations coexist in the relaxed equilibrium state, such illumination or bias induced transitions can drastically change the local net acceptor density.

In the conventional analysis of capacitance experiments, such as deep-level transient spectroscopy, it is assumed that

the transition rate for carrier emission of deep levels behaves as  $\tau^{-1} = \nu_{ee/he} \exp(-\Delta E_{act}/kT)$ , where  $\Delta E_{act}$  is the activation energy of the level, and the prefactor  $\nu_{ee/he}$  (attempt frequency) for the thermal electron or hole emission is the product of the thermal carrier velocity  $V_{th}$ , the effective conduction- or valence-band density of states  $N_{e/h}$ , and the carrier capture cross section  $\sigma$ , i.e.,  $\nu_{ee/he} = V_{th} N_{e/h} \sigma$ . In contrast, transitions which involve activations across an energy barrier in the configuration coordinate diagram are usually described by  $\tau^{-1} = \nu_{ph} \exp(-\Delta E_b/kT)$ , where the  $\nu_{ph}$  is the phonon frequency and  $\Delta E_b$  is the height of the energy barrier in the CCD. (Using the Debye temperature  $T_D = 244 \text{ K}$  in CIS,<sup>46</sup> we obtain  $\nu_{ph} = kT_D/h = 5 \times 10^{12} \text{ s}^{-1}$ .)

Since the donor/acceptor conversion transitions of Eqs. (2) and (3) involve both an energy barrier in the CCD and carrier capture, neither of the two descriptions above are sufficient. However, we can combine the two models in a suitable way to find an expression for the transition rates of Eqs. (2) and (3): Noting that the time window for electron capture in Eq. (2) after a successful activation attempt of the energy barrier  $\Delta E_1$  is in the order of  $1/\nu_{ph}$ ,<sup>47</sup> the probability  $P_{ec}$  of electron capture during one such successful barrier-activation attempt is  $P_{ec} = \nu_{ec}/\nu_{ph}$ , where  $\nu_{ec} = V_{th} n \sigma$  is the electron capture rate analogous to the emission rate  $\nu_{ee}$ , only that the actual electron density  $n$  instead of the effective conduction-band density of states  $N_e$  enters. Thus, the transition rate for the activated electron capture process of Eq. (2) reads

$$\tau_{ec}^{-1} = \nu_{ph} P_{ec} \exp(-\Delta E_1/kT). \quad (4)$$

For the hole capture process, Eq. (3), it is required that two holes be captured during one successful barrier-activation attempt. Therefore, the square of the hole capture probability  $P_{hc} = \nu_{hc}/\nu_{ph}$  enters,

$$\tau_{hc}^{-1} = \nu_{ph} P_{hc}^2 \exp(-\Delta E_2/kT), \quad (5)$$

where the hole capture rate  $\nu_{hc} = V_{th} p \sigma$  depends on the actual hole density  $p$ . From the spatial extension of the  $a$  level (Fig. 4) into which electrons [Eq. (4)] or holes [Eq. (5)] have to be captured, we expect that the capture cross section of this localized level is in the order of  $\sigma = 10 \text{ \AA}^2$ , or  $10^{-15} \text{ cm}^2$ . The rate  $\tau_{he}$  of the hole emission process, i.e., Eq. (3) in the backward direction, is described by a similar expression as Eq. (5), where now the respective barrier for hole emission  $\Delta E_3$  [Table II, Figs. 3(b) and 5(b)] and the square of the hole-emission probability  $P_{he} = \nu_{he}/\nu_{ph}$  enter (with  $\nu_{he}$  as defined above). Once we further determined the electron and hole densities  $n$  and  $p$ , e.g., from the calculated equilibrium Fermi level (see above), all quantities needed for Eqs. (4) and (5) are available, and we will compare the calculated transition rates to experiment in the next section.

## V. THE $(V_{Se}-V_{Cu})$ COMPLEX IN RELATION TO EXPERIMENT

**Light-induced metastability and persistent photoconductivity.** In the  $(V_{Se}-V_{Cu})$  model for metastability, the increase of net  $p$ -type doping after red illumination of CIGS, i.e., the persistent photoconductivity effect, and the accordingly increased junction capacitance of the solar cell,<sup>3-5,8,9,11-14</sup> cor-



respond to the donor-to-acceptor conversion of  $(V_{\text{Se}}-V_{\text{Cu}})$  due to the capture, Eq. (2), of photoexcited electrons. This process is described by the sequence  $1 \rightarrow 2 \rightarrow 3 \rightarrow 4$  in the CCD of Figs. 3(b) and 5(b), and can take place only where the complex existed, at least partly, as  $(V_{\text{Se}}-V_{\text{Cu}})^+$  in the donor configuration before illumination, i.e., at  $d \geq d(-/+)$  in Fig. 6. Since the Fermi level at  $d(-/+)$ ,  $E_F = \varepsilon(+/-)$  (see Table II), is somewhat above the Fermi level in the bulk of the  $p$ -type CIGS absorber, we expect that  $d(-/+)$  is inside, but close to the edge of the space-charge region at room temperature (typically  $\sim 0.5 \mu\text{m}$ ).

Since red illumination excites both electrons and holes in the absorber, the reverse reaction, Eq. (3), i.e., the acceptor-to-donor conversion due to capture of photoexcited holes, could, in principle, take place at the same time. However, due to the larger activation barrier  $\Delta E_2$  (Table II) associated with this transition, and due to the requirement of two holes being captured simultaneously [cf. Eqs. (3) and (5)], the electron capture process is expected to dominate. In addition, since much of the light is absorbed deeper in the absorber,<sup>9</sup> many photoexcited holes never enter the region  $d \leq d(-/+)$  in Fig. 6, where the hole capture, Eq. (3), could take place. Therefore, red illumination can convert most  $(V_{\text{Se}}-V_{\text{Cu}})$  complexes in the active region of the CIGS absorber into the acceptor configuration, thereby increasing the net  $p$  doping and reducing the width of the space charge region. Since the electron capture, Eq. (2), can be initiated either by photoexcited or by electrically generated electrons, the equivalence of red illumination and current injection<sup>2,3,13</sup> is a natural consequence of the  $(V_{\text{Se}}-V_{\text{Cu}})$  model for metastability.

The optical threshold for the red illumination effect and persistent photoconductivity should equal the band gap energy in the  $(V_{\text{Se}}-V_{\text{Cu}})$  model for light-induced metastability (cf. Figs. 3 and 4), being in accord with the observation that the strongest PPC response occurs for illumination above the band edge.<sup>9</sup> A much smaller subgap response was also observed in Ref. 9, which is still consistent with our model if there exist some deep defects allowing for the photo-generation of free electrons by subgap light. The finite energy barrier  $\Delta E_1$  (Table II) in CIS and low-gap CIGS for the electron capture, Eq. (2), should lead to a freeze-out of the red illumination effect at low temperature [cf. Eq. (4)]. Depending on the density of photoexcited electrons the freeze-out should occur around 50 K or somewhat higher temperature. Indeed, it was recently observed in Ref. 15 that the increase in capacitance due to lightsoaking is much less pronounced at  $T=100$  K compared to ambient temperature. In the larger-gap CGS, the unoccupied  $a$  level of the initial  $(V_{\text{Se}}-V_{\text{Cu}})^+$  state is inside the band gap [cf. Table I and Fig. 5(a)], so that photoexcited electrons can be captured according to Eq. (2) without activation in CGS ( $\Delta E_1=0$ , Table I). This leads to the prediction that the red illumination effect can be suppressed at low temperature in CIS, but not in CGS.

Since the blue illumination effect<sup>8</sup> is accompanied by a decrease in junction capacitance, it could be explained in the  $(V_{\text{Se}}-V_{\text{Cu}})$  model by the conversion from the acceptor into the donor configuration due to the hole capture, Eq. (3), which leads to a decreased net acceptor density in the absorber.

Indeed, most photons are absorbed in the CdS buffer during blue illumination,<sup>8</sup> so that most photoexcited electrons do not enter into the CIGS absorber. Consequently, the situation during red illumination is reversed, in that the electron capture, Eq. (2), is suppressed, while the hole capture, Eq. (3), can take place due to the presence of excess holes, which, originally photoexcited in the CdS buffer, are swept into the CIGS absorber. This process requires that  $(V_{\text{Se}}-V_{\text{Cu}})$  existed in the acceptor configuration before blue illumination, and, hence, occurs closer to the junction, i.e., at distances  $d \leq d(-/+)$  in Fig. 6. Further, due to the larger energy barrier  $\Delta E_2$  (Table II) associated with the hole capture process, the blue illumination effect should occur mostly at elevated temperature [cf. Eqs. (3) and (5)].

*Relaxation dynamics of the light-induced metastable state.* The recovery of the equilibrium state after illumination or electron injection occurs generally on the time scale of hours at room temperature.<sup>2,5,9,14</sup> Taking our example from Sec. IV above, where we have  $2.5 \times 10^{16} \text{ cm}^{-3}$  net  $p$ -type doping when all complexes are converted into the acceptor configuration after illumination, we find—in good agreement with the observed time scale—a time constant  $\tau_{\text{hc}} = 10^2 \text{ s}$  [Eq. (5)] for the hole capture, Eq. (3), which leads to the back transition towards the equilibrium state. Note that during the back transition, the hole concentration is reduced, leading to an increasing time constant during the recovery of the equilibrium state. A change in the hole density by a factor of 1/5, as in the example above, implies a 25 times longer time constant  $\tau_h$ , according to Eq. (5). This consequence of our model may, at least partly, explain the nonexponential decay of PPC as observed, e.g., in Ref. 9.

*Reverse-bias metastability.* The main effect of reverse-bias treatment is an increased junction capacitance due to an increased acceptor density,<sup>4,7,8,10,15</sup> like in the case of the red illumination effect. The increase in  $p$ -type doping occurs, however, only in some interval  $0.3 \mu\text{m} \leq d \leq 0.8 \mu\text{m}$  at intermediate distances from the junction. Farther from the junction, at  $d \geq 0.8 \mu\text{m}$ , the net acceptor density may even decrease somewhat upon reverse bias.<sup>4,5,15</sup> Generally speaking, the application of reverse bias increases the width of the space-charge region and depletes electrons and holes. However, at some intermediate distances from the junction, which lie outside the space-charge region before bias but inside the space-charge region during reverse bias, the actual electron concentration can increase from very low levels before bias to higher levels during reverse bias: According to numerical modeling of the CdS/CIGS junction,<sup>48</sup> the electron density may increase from, e.g.,  $n = 10^1 \text{ cm}^{-3}$  to the  $\sim 10^7 \text{ cm}^{-3}$  range around  $d \approx 0.4 \mu\text{m}$ , which approximately coincides with the distance  $d(-/+)$  around which the donor and acceptor configurations of  $(V_{\text{Se}}-V_{\text{Cu}})$  coexist.

The changes in local carrier densities upon reverse bias can lead via two different pathways to the donor-to-acceptor conversion of the  $(V_{\text{Se}}-V_{\text{Cu}})$  complex. In the relaxed state before bias, both Eqs. (2) and (3) are in a steady state with respect to the forward and backward directions, and the donor and acceptor configurations of the complex are of comparable order of magnitude around  $d(-/+)$  (see above). Upon reverse bias, the increased electron density at interme-

diate distances from the junction drives the electron capture, Eq. (2), in the forward direction. Taking  $n=10^7 \text{ cm}^{-3}$ ,<sup>48</sup> we find from Eq. (4) a time constant  $\tau_{ec}=10^2 \text{ s}$  at  $T=300 \text{ K}$ . Second, due to hole depletion, the forward direction of the hole capture, Eq. (3), is suppressed, which drives Eq. (3) in the backward direction, i.e., hole emission, for which we find the time constant  $\tau_{hc}=10^3 \text{ s}$  at  $T=300 \text{ K}$ . Thus, both electron capture and hole emission are expected to lead to an increased acceptor density at intermediate distance from the junction, at the time scale of reverse-bias experiments. These two processes may be discernible by their different energy barriers  $\Delta E_1$  and  $\Delta E_3$  (Table II), which should, to a large extent, determine the apparent activation energy of the bias-induced changes. Note, however, that the transitions, Eqs. (2) and (3), depend on the local electron and hole concentrations, which, in turn, depend on temperature due to a temperature dependent depletion width. This may lead to a contribution to the apparent thermal activation energy, in addition to the barrier height.

The recovery of the equilibrium state after reverse-bias treatment was investigated in Ref. 15 in a thermally stimulated capacitance experiment, by analyzing the (negative) capacitance step after which the increased capacitance of the metastable state relaxed back to the capacitance of the equilibrium state before reverse-bias treatment. In our  $(V_{Se}-V_{Cu})$  model, this step is caused by the back transition from the acceptor into the donor configuration by the hole capture, Eq. (3). The activation energy of 0.32 eV measured in Ref. 15 for this transition compares well with our calculated energy barriers in Table II. Also, the measured frequency prefactor of  $\nu_0=4 \times 10^4 \text{ s}^{-1}$  (Ref. 15) supports the  $(V_{Se}-V_{Cu})$  model, as we find from Eq. (5) a similar value  $\nu_{ph}P_{hc}^2=10^3 \text{ s}^{-1}$  (e.g.,  $T=300 \text{ K}$ ,  $p=10^{16} \text{ cm}^{-3}$ ).

Due to the pinning behavior of the  $(V_{Se}-V_{Cu})$  complex (see above), the complex is expected to exist partly in the acceptor configuration for quite some distance beyond  $d=d(-/+)$  in Fig. 6, at or above room temperature. For such larger distances from the CdS/CIGS heterojunction, e.g., beyond the space-charge region at zero bias, electrons are depleted during reverse bias, which could drive the acceptor-to-donor conversion by Eq. (2) in the backward direction and reduce the net  $p$  doping farther from the junction, as observed in some experiments.<sup>4,5,15</sup> However, this process is expected to be very slow ( $\tau \approx 10^8 \text{ s}$ ) at room temperature and may not be relevant. On the other hand, the acceptor-to-donor conversion by hole capture, Eq. (3), requires that the hole density increases with respect to the zero bias conditions at these farther distances. Such an increased hole density may be explained as a consequence of the increased acceptor density at intermediate distances. Taking a hole density of  $p=10^{16} \text{ cm}^{-3}$ , we find a time constant  $\tau_{hc}=10^2 \text{ s}$  at  $T=300 \text{ K}$ , which is again within the time scale of reverse-bias experiments. Thus, due to the different situations close and far from the CdS/CIGS heterojunction, the amphoteric behavior of the  $(V_{Se}-V_{Cu})$  complex could explain the simultaneous increase and decrease of the net acceptor density closer and farther from the junction, respectively. The as-

sumption of reversible long-range atomic diffusion, as proposed in Refs. 4 and 5 is not necessary to explain the experimental observations.

*Red-on-bias metastability.* The combination of reverse bias and red illumination (red-on-bias) creates a particular metastable state, different from those described above.<sup>49</sup> In this state, the depletion width of the CdS/CIGS heterojunction is strongly reduced, presumably due to a large amount of electrons of up to  $10^{18} \text{ cm}^{-3}$ , captured into a deep state very close to the junction.<sup>49</sup> The fact the these electrons are not released below 300 K creates an apparent paradox: On the one hand, the level must be close to the CBM, so that it is empty before the red-on-bias treatment. On the other hand, it must be deep, i.e., in the lower part of the gap, so that electrons remain in the level up to 300 K. In order to resolve the paradox one has to assume a defect which, first, has an equilibrium transition level close to the CBM, second, creates a defect-localized-state in the lower part of the gap after electron capture (e.g., following a large lattice relaxation), and, third, has a large energy barrier for electron reemission into the conduction band. While the  $\varepsilon(-/2-)$  and  $\varepsilon(2-/3-)$  transition levels of  $(V_{Se}-V_{Cu})$  fulfill the first requirement, the occupation of the  $b$  level [Figs. 3(a), 4, and 5(a)] does not lead to a defect state in the lower part of the CIGS gap, and an energy barrier for electron-emission from the  $b$  level into the CBM is also not present. Thus, the red-on-bias effect is one kind of metastability that cannot be explained in the  $(V_{Se}-V_{Cu})$  model. Further studies towards the nature of the defect responsible for this effect are being pursued.

*Deep levels related to metastability.* After electron injection, a deep hole trap at 0.26 eV above the VBM was reported in Ref. 2 to appear in the metastable state. However, metastable behavior is not necessarily associated with the appearance of this level. In particular, more “modern” CIGS solar cells do usually not show this level in the metastable state,<sup>15</sup> despite the fact that metastability occurs in a very similar fashion compared to the older experiments of Ref. 2. This indicates that the 0.26 eV hole trap is not directly caused by the metastable defects (cf. Ref. 39), but rather belongs to a different defect, and appears only due to indirect changes associated with metastability, e.g., the increased net doping. A deep trap showing a strong correlation with light-induced metastability has also been reported in Refs. 11–13. Whether this trap could be related to the  $(V_{Se}-V_{Cu})$  complex itself, e.g., to the deep  $\varepsilon(-/2-)$  acceptor state, or whether it is rather an indirect effect like in the case of the 0.26 eV hole trap above is presently not clear. Further, there is a prominent capacitance step observed in thermally stimulated capacitance experiments which occurs, e.g., around 250 K at a test frequency of 100 kHz.<sup>4,7,8,15</sup> This capacitance step is often also present in the relaxed state, but it increases considerably in the metastable state after reverse-bias treatment. Igalson *et al.*<sup>10,15</sup> suggested that this capacitance step may be caused by defect levels that are high in the gap and intersect the Fermi level close to the junction. While such defect levels not necessarily need to originate from the metastable defect itself, we note that the  $(V_{Se}-V_{Cu})$  does produce such levels, i.e., the deep  $\varepsilon(-/2-)$  and  $\varepsilon(2-/3-)$  acceptor transitions [see Figs. 2(a) and 6].

*Can the amphoteric ( $V_{\text{Se}}-V_{\text{Cu}}$ ) defect explain unusual capacitance transients?* Even though the dynamics of the activated  $\varepsilon(+/-)$  transition corresponding to the donor/acceptor conversion of ( $V_{\text{Se}}-V_{\text{Cu}}$ ) is different from conventional transitions (cf. Sec. IV), this conversion may be—in both directions—observed directly in capacitance experiments, proposed the temperature, and frequency windows are appropriate. [Note that in the experiments cited above, the evidence for the  $\varepsilon(+/-)$  transition of ( $V_{\text{Se}}-V_{\text{Cu}}$ ) is only indirect and is manifested by a change of the shallow acceptor concentrations due to illumination or bias. The shallow acceptor density is usually determined at low temperature, where the  $\varepsilon(+/-)$  transition itself is not activated.] Recently, Young *et al.*<sup>16</sup> and Young and Crandall<sup>17</sup> observed unusual capacitance transients due to electron and hole traps, measured at comparatively high temperatures of 380–400 K. In these experiments, a filling pulse of zero or small forward bias is applied, and the capacitance is measured subsequently as a function of time under reverse bias, yielding the frequency prefactor and the activation energy of the observed transitions. The measured frequency prefactors deviated largely from expectations, and were unusual in that the transition with a larger activation energy occurred faster, due to a larger prefactor.<sup>16,17</sup> In order to reconcile the observed transitions with transition rate theory, large entropy changes were postulated in Refs. 16 and 17 to be associated with the transitions.

In such capacitance-transient experiments, the donor-to-acceptor conversion of ( $V_{\text{Se}}-V_{\text{Cu}}$ ) by the electron capture, Eq. (2), would appear like a hole trap which causes a capacitance increase when holes are emitted. Also, the donor-to-acceptor conversion by hole emission, i.e., Eq. (3) in the backward direction, would appear as a hole trap, and the faster transition would dominate the hole trap signal. While, at the lower temperature  $T=300$  K, the electron capture is the faster transition (see above), at the higher temperatures used in the experiments of Refs. 16 and 17, e.g.,  $T=380$  K, the hole emission is faster [ $\tau_{\text{he}}=10^{-1}$  s calculated from Eq. (5)] than the electron capture [ $\tau_{\text{ec}}=10$  s calculated from Eq. (4) for  $n=10^7$  cm<sup>-3</sup> as above]. This crossover in the transition rates is a consequence of the different energy barriers of the electron capture ( $\Delta E_1$ ) and hole emission ( $\Delta E_3$ ) processes. Note that indeed two different hole traps are observed in Refs. 16 and 17 at lower (e.g., 300 K) and higher (e.g., 380 K) temperatures. Next, the acceptor-to-donor transition by hole capture, Eq. (3) in the forward direction, will in such capacitance transient experiments appear like an electron trap which causes a capacitance decrease when electrons are emitted. Considering that this transition should happen deeper in the absorber where the hole density is essentially bulklike (see above), we take, e.g.,  $p=10^{16}$  cm<sup>-3</sup> and obtain a time constant  $\tau_{\text{hc}}=1$  s at  $T=380$  K, for the electron trap signal.

While the energy barriers corresponding to the hole trap signal ( $\Delta E_1$  and  $\Delta E_3$ ) and the barrier corresponding to the electron trap signal ( $\Delta E_2$ ) do not agree with the activation energies observed in Refs. 16 and 17, the respective time constants  $\tau_{\text{he}}=10^{-1}$  s and  $\tau_{\text{hc}}=1$  s, calculated from Eqs. (4) and (5), agree reasonably, i.e., within one to two orders of magnitude, with the measured time constants at  $T=380$  K.

[Note, again, that the apparent activation energies of the donor/acceptor conversion of ( $V_{\text{Se}}-V_{\text{Cu}}$ ) may deviate from the respective energy barriers, because of the temperature dependent local carrier density.] Therefore, the ( $V_{\text{Se}}-V_{\text{Cu}}$ ) model reasonably explains the observed capacitance transients and, notably, accounts for the two different hole trap signals being observed at different temperatures. Further, it is interesting to note that the finite capture/emission probabilities per successful barrier-activation attempt, i.e.,  $P_{\text{ec}}$  in Eq. (4) and  $P_{\text{he}}^2$  or  $P_{\text{he}}^2$  in Eq. (5), can be cast as an entropy factor, e.g.,  $P_{\text{ec}}=\exp(\Delta S/k)$ , which alters the effective frequency prefactor with respect to the phonon frequency  $\nu_{\text{ph}}$  [cf. Eqs. (4) and (5)]. Thus, our ( $V_{\text{Se}}-V_{\text{Cu}}$ ) model may provide a physical interpretation of the entropy changes that were postulated as abstract quantities in Ref. Ref. 16 and 17.

*Correlation between metastability and stoichiometry.* Experimentally, the sample stoichiometry appears to correlate with light-induced metastability: Comparing In- and Cu-rich grown CIS solar cells, it was found in Ref. 4 that only the In-rich sample showed the increased low temperature capacitance which is characteristic of the PPC effect. From the calculated CIS and CGS phase diagrams, we have found before<sup>30</sup> that the maximally In-rich growth conditions (maximal  $\Delta\mu_{\text{In}}$ ) correspond, at the same time, also to maximally Se-poor conditions (minimal  $\Delta\mu_{\text{Se}}$ ). Thus, while  $V_{\text{Cu}}$  should be abundant under any growth condition,<sup>31,32</sup> we expect that considerable  $V_{\text{Se}}$  concentrations, and, hence, the formation of ( $V_{\text{Se}}-V_{\text{Cu}}$ ) complexes, should occur mostly in In-rich grown material. Further, the formation of ( $V_{\text{Se}}-V_{\text{Cu}}$ ) in In-rich material and the suppression of it in Cu-rich material are consistent with the conclusion of Refs. 50 and 51, where a defect observed by positron annihilation spectroscopy has been assigned to the ( $V_{\text{Se}}-V_{\text{Cu}}$ ) complex, and where it was found that the formation of this defect is suppressed in Cu-rich growth conditions, as indicated by the presence of a  $\text{Cu}_x\text{Se}$  secondary phase. Thus, we conclude that metastability due to the ( $V_{\text{Se}}-V_{\text{Cu}}$ ) complex should be controllable by the absorber growth conditions.

*Optical recombination centers.* In pure CIS and lower Ga-content CIGS, the  $a$  and  $b$  levels of the ( $V_{\text{Se}}-V_{\text{Cu}}$ )<sup>+</sup> donor configuration are resonant inside the conduction band (Fig. 3), and do not cause optical absorption or luminescence. In the acceptor configuration of ( $V_{\text{Se}}-V_{\text{Cu}}$ ), however, which is present within  $d<d(-/+)$  in Fig. 6, the empty  $b$  level lies inside the band gap [Table I and Fig. 3(a)], and could act as a recombination center causing losses in a photovoltaic device. We calculated the optical absorption energy  $E_{\text{abs}}$  corresponding to the excitation of an electron from the VBM into the  $b$  level ( $a^2b^0 \rightarrow a^2b^1+h$ ), as well as the luminescence energy  $E_{\text{PL}}$  corresponding to the recombination of an electron in the  $b$  level with a hole at the VBM ( $a^2b^1+h \rightarrow a^2b^0$ ). We see in Table II that the absorption energy  $E_{\text{abs}}$  between 1.0 and 1.2 eV, and the PL energy  $E_{\text{PL}}$  around 0.9 eV change little between CIS and CGS.

Recent optical experiments in CIGS alloys<sup>21–23</sup> have found an absorption level between 0.8 and 1.0 eV showing practically no variation with the Ga content between  $x=0.0$  and  $x=0.8$ .<sup>21</sup> The invariance against the Ga composition, and, hence, the band gap of the CIGS alloy, is a striking



similarity with our calculated absorption level of ( $V_{\text{Se}}-V_{\text{Cu}}$ ), indicating that this complex could be the origin of the observed levels. Further, the defect assigned in Ref. 50 to ( $V_{\text{Se}}-V_{\text{Cu}}$ ) on basis of positron lifetimes showed a correlation with a PL band around 0.85 eV, close to our calculated PL energies in Table II. Contrasting with the identification of ( $V_{\text{Se}}-V_{\text{Cu}}$ ) as the origin of the optical levels, the absorption levels observed in Ref. 23 have been attributed to the intrinsic  $\text{In}_{\text{Cu}}$  donor, based on older calculations<sup>31,42</sup> which found rather deep donor transition energies for  $\text{In}_{\text{Cu}}$ . However, more recent calculations<sup>29,30,32</sup> which employ all the corrections to LDA energies described in Sec. II, yield shallow levels for  $\text{In}_{\text{Cu}}$ , and identify this defect as the source of intrinsic  $n$ -type conductivity, which can be obtained in CIS under appropriate growth conditions. Hence, from the theoretical point of view, the ( $V_{\text{Se}}-V_{\text{Cu}}$ ) complex may still be the more reasonable candidate for the absorption levels.

*Is metastability a concern for device performance?* The importance of the above discussed optical levels as recombination centers has been highlighted in Ref. 21, in particular, with view to its detrimental effects in larger-gap CIGS alloys. Attributing the observed optical levels to the  $b$  level [Figs. 3(a), 4, and 5(a)] of ( $V_{\text{Se}}-V_{\text{Cu}}$ ) in the acceptor configuration raises indeed concerns about the presence of these metastable defects in CIGS based solar cells: Once the difference between electron and hole Fermi levels raises above the  $\varepsilon(-/2-)$  transition around 1 eV [Fig. 2(a)], e.g., under open circuit conditions, the recombination of electrons trapped in the  $b$  level with free holes must be expected to limit the open circuit voltage  $V_{\text{oc}}$ . The invariance of this transition energy with the Ga content of the CIGS alloy may then lead to the saturation of  $V_{\text{oc}}$  with increasing CIGS band gap,<sup>52</sup> possibly in connection with Fermi-level pinning in CIGS due to  $V_{\text{Cu}}$  formation.<sup>30</sup> On the other hand, the ( $V_{\text{Se}}-V_{\text{Cu}}$ ) model may also lead to an interpretation of the beneficial effect of light soaking.<sup>4,7,8,10</sup> Illumination with “white” light should result in a superposition of the red and blue illumination effects discussed above. While the red illumination effect has the beneficial effect of increasing the net acceptor density deeper in the absorber, it also has the detrimental effect of increasing the number of recombination centers caused by the ( $V_{\text{Se}}-V_{\text{Cu}}$ ) complex in the acceptor configuration. The blue illumination effect being present at the same time may have the beneficial effect of back converting the ( $V_{\text{Se}}-V_{\text{Cu}}$ ) complex into the donor configuration closer to the junction, thereby decreasing the number of recombination centers at shorter distances from the junction, i.e., where recombination centers are developing the strongest detrimental effect. Still, the overall beneficial effect of light soaking may actually result only from a balance of beneficial (increased space charge density) and detrimental (recombination centers) effects, and the presence of metastable defects should be regarded as a concern for the efficiency of CIGS solar cells.

## VI. CONCLUSION

We found from first-principles total-energy calculations that the ( $V_{\text{Se}}-V_{\text{Cu}}$ ) complex in CIS and CGS exhibits meta-

stable and amphoteric behavior. Using additional modeling for the equilibrium thermodynamics and the transition dynamics after creation of a metastable nonequilibrium state, we were able to relate the theoretical results to a large number of experiments, and to establish a comprehensive model for metastability caused by the ( $V_{\text{Se}}-V_{\text{Cu}}$ ) complex, suggesting that both light-induced and bias-induced metastabilities originate from this defect. The presence of recombination centers in one of the two ( $V_{\text{Se}}-V_{\text{Cu}}$ ) configurations highlights concerns about the presence of metastable defects for the device performance.

## ACKNOWLEDGMENTS

This work was funded by the U.S. Department of Energy, Office of Energy Efficiency and Renewable Energy, under Contract No. DE-AC36-99GO10337 to NREL. Also, the authors acknowledge illuminating and continued discussions with M. Igalson (Warsaw University) and J. D. Cohen (University of Oregon).

- <sup>1</sup>M. N. Ruberto and A. Rothwarf, J. Appl. Phys. **61**, 4662 (1987).
- <sup>2</sup>M. Igalson and H. W. Schock, J. Appl. Phys. **80**, 5765 (1996).
- <sup>3</sup>U. Rau, M. Schmitt, J. Parisi, W. Riedl, and F. Karg, Appl. Phys. Lett. **73**, 223 (1998).
- <sup>4</sup>U. Rau, A. Jasenek, R. Herberholz, H. W. Schock, J. F. Guillemoles, D. Lincot, and L. Kronik, in Proceedings of the Second World Conference on Photovoltaic Energy Conversion (E.C. Joint Res. Centre, Luxembourg, 1998), p. 428.
- <sup>5</sup>R. Herberholz et al., Eur. Phys. J.: Appl. Phys. **6**, 131 (1999).
- <sup>6</sup>Th. Meyer, M. Schmidt, F. Engelhard, J. Parisi, and U. Rau, Eur. Phys. J.: Appl. Phys. **8**, 43 (1999).
- <sup>7</sup>U. Rau, K. Weinert, Q. Nguyen, M. Mamor, G. Hanna, A. Jasenek, and H. W. Schock, Mater. Res. Soc. Symp. Proc. **668**, H.9.1.1 (2001).
- <sup>8</sup>P. Zabierowski, U. Rau, and M. Igalson, Thin Solid Films **387**, 147 (2001).
- <sup>9</sup>Th. Meyer, F. Engelhardt, J. Parisi, and U. Rau, J. Appl. Phys. **91**, 5093 (2002).
- <sup>10</sup>M. Igalson, M. Bodegard, L. Stolt, and A. Jasenek, Thin Solid Films **431–432**, 153 (2003).
- <sup>11</sup>J. T. Heath, J. D. Cohen, and W. N. Shafarman, Thin Solid Films **431–432**, 426 (2003).
- <sup>12</sup>J. T. Heath, J. D. Cohen, and W. N. Shafarman, J. Appl. Phys. **95**, 1000 (2004).
- <sup>13</sup>J. W. Lee, J. T. Heath, D. Cohen, W. N. Shafarman, Mater. Res. Soc. Symp. Proc. **865**, F.12.4.1 (2005).
- <sup>14</sup>J. W. Lee, J. D. Cohen, and W. N. Shafarman, Thin Solid Films **480–481**, 336 (2005).
- <sup>15</sup>M. Igalson, M. Cwil, and M. Edoff, Proceedings of 20th European Photovoltaic Solar Energy Conference (WIP-Renewable Energies, München, 2005), p. 180.
- <sup>16</sup>D. L. Young, K. Ramanathan, and R. S. Crandall, Proceedings of 31st IEEE Photovoltaic Specialists Conference (IEEE, Orlando, 2005), p. 259.
- <sup>17</sup>D. L. Young and R. S. Crandall, Appl. Phys. Lett. **86**, 262107 (2005).
- <sup>18</sup>K. Gartsman et al., J. Appl. Phys. **82**, 4282 (1997).
- <sup>19</sup>S. Lany and A. Zunger, Phys. Rev. Lett. **93**, 156404 (2004).
- <sup>20</sup>S. Lany and A. Zunger, Phys. Rev. B **72**, 035215 (2005).
- <sup>21</sup>J. T. Heath, J. D. Cohen, W. N. Shafarman, D. X. Liao, and A. A. Rockett, Appl. Phys. Lett. **80**, 4540 (2002).
- <sup>22</sup>Y. Akaki et al., Thin Solid Films **480–481**, 250 (2005).
- <sup>23</sup>M. Igalson and M. Edoff, Thin Solid Films **480–481**, 322 (2005).
- <sup>24</sup>J. Ihm, A. Zunger, and M. L. Cohen, J. Phys. C **12**, 4409 (1979).
- <sup>25</sup>D. M. Ceperley and B. J. Alder, Phys. Rev. Lett. **45**, 566 (1980).
- <sup>26</sup>J. P. Perdew and A. Zunger, Phys. Rev. B **23**, 5048 (1981).
- <sup>27</sup>P. E. Blöchl, Phys. Rev. B **50**, 17953 (1994); G. Kresse and J. Furthüller, Comput. Mater. Sci. **6**, 15 (1996); G. Kresse and J. Joubert, Phys. Rev. B **59**, 1758 (1999).
- <sup>28</sup>In principle, neither the experimental nor the LDA equilibrium lattice constant (usually smaller than the real lattice constant) represents an optimal situation. The choice of the LDA (equilibrium) lattice constant implies

an overestimated overlap and, hence, interaction between defect and host orbitals, whereas the choice of the experimental (nonequilibrium) lattice constant implies the presence of some hydrostatic pressure acting on the lattice in the calculation. Fortunately, there are usually only minor differences in the defect formation and transition energies. Since the large lattice relaxation of the anion vacancies in II-VI compounds is particularly sensitive to the lattice constant (Ref. 20) the differences can be more pronounced, in the case of anion vacancies, however. For CIS and CGS, we confirmed by additional calculations that  $\Delta H$  changes by not more than 0.2 eV when using the LDA lattice constant.

- <sup>29</sup>S. Lany, Y. J. Zhao, C. Persson, and A. Zunger, Appl. Phys. Lett. **86**, 042109 (2005).
- <sup>30</sup>Y. J. Zhao, C. Persson, S. Lany, and A. Zunger, Appl. Phys. Lett. **85**, 5860 (2004).
- <sup>31</sup>S. B. Zhang, S. H. Wei, A. Zunger, and H. Katayama-Yoshida, Phys. Rev. B **57**, 9642 (1998).
- <sup>32</sup>C. Persson, Y. J. Zhao, S. Lany, and A. Zunger, Phys. Rev. B **72**, 035211 (2005).
- <sup>33</sup>V. I. Anisimov, I. V. Solovyev, M. A. Korotin, M. T. Czyzyk, and G. A. Sawatzky, Phys. Rev. B **48**, 16929 (1993); A. I. Liechtenstein, V. I. Anisimov, and J. Zaanen, *ibid.* **52**, R5467 (1995).
- <sup>34</sup>M. Usuda, N. Hamada, T. Kotani, and M. van Schilfgaarde, Phys. Rev. B **66**, 125101 (2002).
- <sup>35</sup>L. Hedin and S. Lundqvist, in *Solid State Physics*, edited by F. Seitz, D. Turnbull, and H. Ehrenreich (Academic, New York, 1969), Vol. 23, p. 1.
- <sup>36</sup>H. Weinert, H. Neumann, H. J. Höbner, G. Kühn, and N. Van Nam, Phys. Status Solidi B **81**, K59 (1977).
- <sup>37</sup>T. Irie, S. Endo, and S. Kimura, Jpn. J. Appl. Phys. **18**, 1303 (1979).
- <sup>38</sup>We determined  $m_h^*/m_e=0.8$  from fitting an effective-mass-like density of states (degeneracy factor of 2) to the numerical density of states, calculated in LDA including spin-orbit coupling. The obtained value is close to  $m_h^*/m_e=0.73$  determined experimentally in Ref. 37.
- <sup>39</sup>In Ref. 20, we determined  $\Delta V$  from the difference of the single-particle energy of the In-*d* (Ga-*d*) orbitals in the defect calculation relative to In-*d* (Ga-*d*) energy in the pure host. The present method appears to yield more consistent results and less uncontrolled scatter compared to the former method. Accordingly, the potential alignment  $\Delta V$  for the

( $V_{Se}-V_{Cu}$ ) complex determined here differs by up to 0.2 eV from that determined in Ref. 20. The most significant change is that we now find a shallow state of the acceptor configuration of ( $V_{Se}-V_{Cu}$ ), similar to the shallow state of the isolated  $V_{Cu}$  (see Table I). Before, we found a deeper state  $\varepsilon(0/-)=E_V+0.27$  eV (Ref. 20) for the complex. Further, the deep acceptor levels of the isolated  $V_{Se}$  now appear as closely spaced, but separate  $\varepsilon(0/-)$  and  $\varepsilon(-/2-)$  levels, whereas we found a weak negative-*U* behavior and a  $\varepsilon(0/2-)$  transition before. (Ref. 20).

- <sup>40</sup>G. Makov and M. C. Payne, Phys. Rev. B **51**, 4014 (1995).
- <sup>41</sup>U. Gerstmann, P. Deák, R. Rurali, B. Aradi, Th. Frauenheim, and H. Overhof, Physica B **340-342**, 190 (2003).
- <sup>42</sup>S. H. Wei, S. B. Zhang, and A. Zunger, Appl. Phys. Lett. **72**, 3199 (1998).
- <sup>43</sup>J. F. Guilleminot, U. Rau, L. Kronik, H. W. Schock, and D. Cahen, Adv. Mater. (Weinheim, Ger.) **11**, 957 (1999).
- <sup>44</sup>Figure 4 was created with the visual molecular dynamics (vmd) package; W. Humphrey, A. Dalke, and K. Schulten, J. Mol. Graphics **14**, 33 (1996).
- <sup>45</sup>The energy barriers  $\Delta E_1$ ,  $\Delta E_2$ , and  $\Delta E_3$  are actually determined for the isolated  $V_{Se}$ . Since energies of the *a* and *b* defect levels and the mechanism of III-III bond formation/breakup that leads to the barriers is hardly affected upon complex formation with  $V_{Cu}$ , the respective energies for ( $V_{Se}-V_{Cu}$ ) are expected to be very similar.
- <sup>46</sup>B. Fernandez and S. M. Wasim, Phys. Status Solidi A **122**, 235 (1990).
- <sup>47</sup>For the electron capture, Eq. (2), the empty *a* level needs to be activated to energies below the CBM. Similarly, for the hole capture, Eq. (3), the occupied *a* level must be activated to energies above the VBM. This happens only for some fraction of the time  $1/\nu_{ph}$  needed for a full oscillation around the local minima in the CCD [Figs. 3(b) and 5(b)].
- <sup>48</sup>M. Igalson (private communication).
- <sup>49</sup>M. Igalson, M. Bodegard, and L. Stolt, Sol. Energy Mater. Sol. Cells **80**, 195 (2003).
- <sup>50</sup>S. Niki, R. Suzuki, S. Ishibashi, T. Ohdaira, P. J. Fons, A. Yamada, H. Oyanagi, T. Wada, R. Kimura, and T. Nakada, Thin Solid Films **387**, 129 (2001).
- <sup>51</sup>S. Niki, A. Yamada, R. Hunger, P. J. Fons, K. Iwata, K. Matsubara, A. Nishio, and H. Nakanishi, J. Cryst. Growth **237-239**, 1993 (2002).
- <sup>52</sup>W. N. Shafarman, R. Klenk, and B. E. McCandless, J. Appl. Phys. **79**, 7324 (1996).